International Standard

ISO 27852

Space systems — Estimation of orbit lifetime

Systèmes spatiaux — Estimation de la durée de vie en orbite

Third edition
2024-02

Reference number
ISO 27852:2024(en)

ISO copyright office
CP 401 • Ch. de Blandonnet 8
CH-1214 Vernier, Geneva
Phone: +41 22 749 01 11
Email: copyright@iso.org
Website: www.iso.org

Published in Switzerland

Contents

Page

Foreword

ISO (the International Organization for Standardization) is a worldwide federation of national standards bodies (ISO member bodies). The work of preparing International Standards is normally carried out through ISO technical committees. Each member body interested in a subject for which a technical committee has been established has the right to be represented on that committee. International organizations, governmental and non-governmental, in liaison with ISO, also take part in the work. ISO collaborates closely with the International Electrotechnical Commission (IEC) on all matters of electrotechnical standardization.

The procedures used to develop this document and those intended for its further maintenance are described in the ISO/IEC Directives, Part 1. In particular, the different approval criteria needed for the different types of ISO document should be noted. This document was drafted in accordance with the editorial rules of the ISO/IEC Directives, Part 2 (see www.iso.org/directives).

ISO draws attention to the possibility that the implementation of this document may involve the use of (a) patent(s). ISO takes no position concerning the evidence, validity or applicability of any claimed patent rights in respect thereof. As of the date of publication of this document, ISO had not received notice of (a) patent(s) which may be required to implement this document. However, implementers are cautioned that this may not represent the latest information, which may be obtained from the patent database available at www.iso.org/patents. ISO shall not be held responsible for identifying any or all such patent rights.

Any trade name used in this document is information given for the convenience of users and does not constitute an endorsement.

For an explanation of the voluntary nature of standards, the meaning of ISO specific terms and expressions related to conformity assessment, as well as information about ISO's adherence to the World Trade Organization (WTO) principles in the Technical Barriers to Trade (TBT), see www.iso.org/iso/foreword.html.

This document was prepared by Technical Committee ISO/TC 20, *Aircraft and space vehicles*, Subcommittee SC 14, *Space systems and operations*.

This third edition cancels and replaces the second (ISO 27852:2016) edition, which has been technically revised.

The main changes are as follows:

— clarified that this document does not apply to non-LEO protected regions (e.g. GEO);

— harmonized terms and definitions with those in ISO 24113;

— updated to harmonize with IADC [1] and United Nations [2] –[3] guidelines;

— added a subclause on the use of the recommended solar forcing dataset for the Coupled Model Intercomparison Project 6.

Any feedback or questions on this document should be directed to the user’s national standards body. A complete listing of these bodies can be found at www.iso.org/members.html.

Introduction

Constraining estimated orbit lifetime of human-made objects is increasingly important as space debris continues to increase (as documented in Annex A) and as such is one of the central tenets of the global space debris mitigation strategy. This document is a supporting document to ISO 24113, its derivative spacecraft disposal standard ISO 23312 and launch vehicle upper stage disposal technical report ISO/TR 20590. The purpose of this document is to provide a common, consensus-based approach to determining orbit lifetime, one that is sufficiently precise and easily implemented for the purpose of demonstrating conformity with ISO 24113. This document offers standardized guidance and analysis methods to estimate orbital lifetime for all LEO-crossing orbit classes. This document only deals with orbit lifetime issues (orbit decay out of orbits crossing the LEO protected region); for other important requirements related to how long a space object will, or will not, cross or occupy a protected region, the user is directed to ISO 24113 and its derivative ISO 23312.

Space systems — Estimation of orbit lifetime

1 Scope

This document describes a process for the long-duration orbit lifetime prediction of orbit lifetime for spacecraft, launch vehicles, upper stages and associated debris in LEO-crossing orbits after mission phase (including any mission lifetime extensions).

The document also clarifies:

a) modelling approaches and resources for solar and geomagnetic activity modelling;

b) resources for atmosphere model selection;

c) approaches for spacecraft ballistic coefficient estimation.

2 Normative references

The following documents are referred to in the text in such a way that some or all of their content constitutes requirements of this document. For dated references, only the edition cited applies. For undated references, the latest edition of the referenced document (including any amendments) applies.

ISO 24113, *Space systems — Space debris mitigation requirements*

3 Terms, definitions, symbols and abbreviated terms

3.1 Terms and definitions

For the purposes of this document, the following terms and definitions apply.

ISO and IEC maintain terminology databases for use in standardization at the following addresses:

— ISO Online browsing platform: available at https://www.iso.org/obp

— IEC Electropedia: available at https://www.electropedia.org/

3.1.1
disposal
actions performed by a *spacecraft* (3.1.22) or *launch vehicle orbital stage* (3.1.9) to permanently reduce its chance of accidental break-up and to achieve its required long-term clearance of the *protected regions* (3.1.17)

Note 1 to entry: Actions can include removing stored energy and performing post-mission orbital manoeuvres.

3.1.2
disposal phase
interval between the *end of mission* (3.1.5) of a *spacecraft* (3.1.22) or *launch vehicle orbital stage* (3.1.9) and its *end of life* (3.1.4)

3.1.3
Earth orbit
bound or unbound Keplerian *orbit* (3.1.14) with Earth at a focal point, or Lagrange point orbit which includes Earth as one of the two main bodies

3.1.4
end of life
instant when a *spacecraft* (3.1.22) or *launch vehicle orbital stage* (3.1.9):

a) is permanently turned off, nominally as it completes its *disposal phase* (3.1.2),

b) completes its manoeuvres to perform a *controlled re-entry* (3.1.18) into the Earth's atmosphere, or

c) can no longer be controlled by the operator

3.1.5
end of mission
instant when a *spacecraft* (3.1.22) or *launch vehicle orbital stage* (3.1.9):

a) completes the tasks or functions for which it has been designed, other than its *disposal* (3.1.1),

b) becomes incapable of accomplishing its *mission* (3.1.12), or

c) has its *mission* (3.1.12) permanently halted through a voluntary decision

3.1.6
GEO
Earth orbit (3.1.3) having zero inclination, zero eccentricity, and an orbital period equal to the Earth's sidereal rotation period

3.1.7
high area-to-mass
having a ratio of area to mass exceeding 0,1 m^2/kg

3.1.8
launch vehicle
DEPRECATED: launcher
system designed to transport one or more payloads into outer space

3.1.9
launch vehicle orbital stage
complete element of a *launch vehicle* (3.1.8) that is designed to deliver a defined thrust during a dedicated phase of the launch vehicle's operation and achieve *orbit* (3.1.14)

Note 1 to entry: Non-propulsive elements of a launch vehicle, such as jettisonable tanks, multiple payload structures or dispensers, are considered to be part of a launch vehicle orbital stage while they are attached.

3.1.10
LEO-crossing orbit
orbit (3.1.14) having perigee within the LEO protected zone, i.e. with perigee altitude of 2 000 km or less

Note 1 to entry: As shown in Figure A.3, orbits having this definition encompass the majority of the high spatial density spike of *spacecraft* (3.1.22) and *space debris* (3.1.20).

3.1.11
long-duration orbit lifetime prediction
orbit lifetime (3.1.15) prediction spanning two *solar cycles* (3.1.19) or more (e.g. 25-year orbit lifetime)

3.1.12
mission
set of tasks or functions to be accomplished by a *spacecraft* (3.1.22) or *launch vehicle orbital stage* (3.1.19), other than its *disposal* (3.1.1)

3.1.13
mission phase
phase where the space system fulfils its *mission* (3.1.12), beginning at the end of the launch phase and ending when the space system no longer performs its intended mission or purpose

3.1.14
orbit
regular recurring path that a *space object* (3.1.21) takes about its primary attracting body

3.1.15
orbit lifetime
elapsed time between the orbiting *spacecraft's* (3.1.22) initial or reference position and its *re-entry* (3.1.18)

Note 1 to entry: Examples of "initial position" are the injection into *orbit* (3.1.14) of a spacecraft or *launch vehicle orbital stage* (3.1.9), or the instant when *space debris* (3.1.20) is generated. An example of a "reference position" is the orbit of a spacecraft or launch vehicle orbital stage at the *end of mission* (3.1.5).

Note 2 to entry: The orbit's decay is typically represented by the reduction in perigee and apogee altitudes (or radii) as shown in Figure 1.

Note 3 to entry: Ballistic flight re-entry typically begins at 25 km to 50 km altitude.

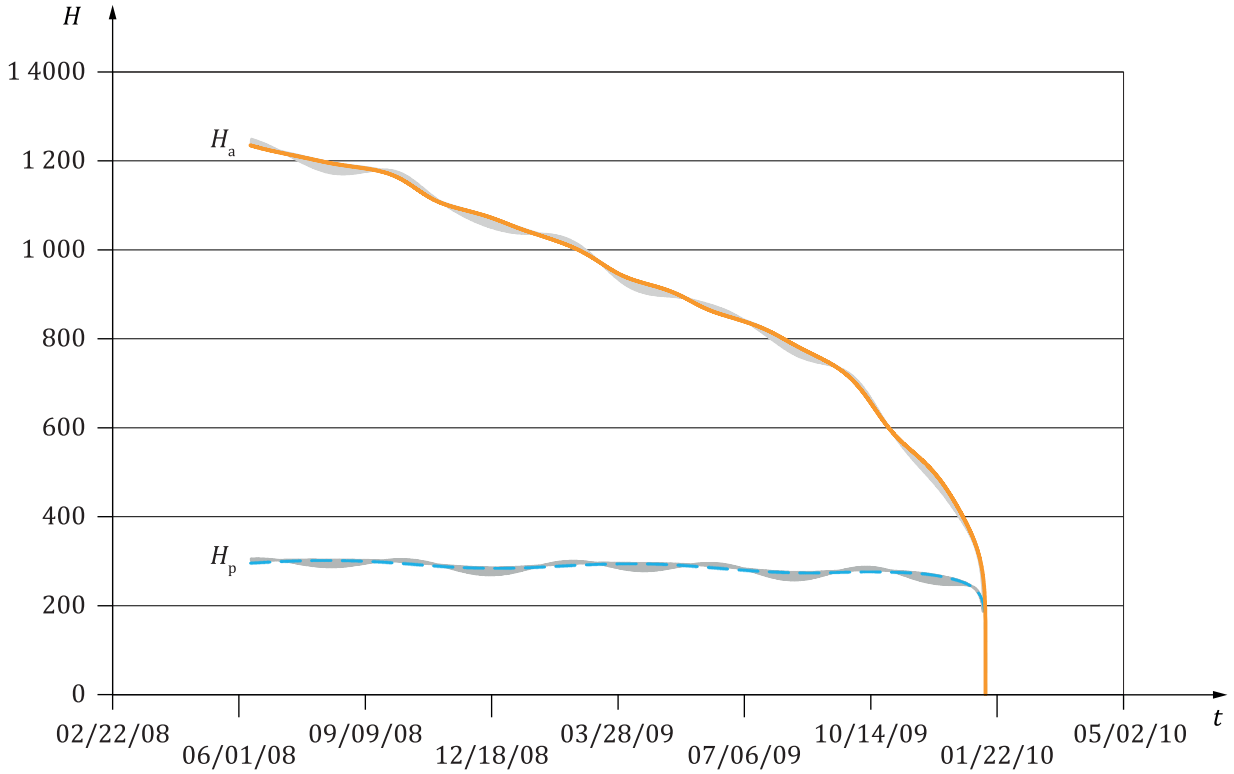

Key

t time, expressed as calendar date
H_a apogee height, expressed in km
H_p perigee height, expressed in km

Figure 1 — Sample of orbit lifetime perigee and apogee decay profile

3.1.16
post-mission orbit lifetime
duration of the *orbit* (3.1.14) after completion of the *mission phase* (3.1.13)

Note 1 to entry: The *disposal phase* (3.1.2) duration is a component of the post-mission duration.

3.1.17
protected region
region in outer space that is protected with regard to the generation of *space debris* (3.1.20) to ensure its safe and sustainable use in the future

3.1.18
re-entry
permanent return of a *space object* (3.1.21) into the Earth's atmosphere

Note 1 to entry: Several alternative definitions are available for the delineation of a boundary between the Earth's atmosphere and outer space.

3.1.19
solar cycle
≈11-year time period which encompasses the 13-month oscillatory variation of solar radio flux, as observed by monthly sunspot number and highly correlated with the 13-month running mean of measurements taken at the 10,7 cm wavelength

Note 1 to entry: Historical records back to the earliest recorded data (1945) are shown in Figure 2.

Note 2 to entry: For reference, the 25-year *post-mission orbit lifetime* (3.1.16) constraint specified in ISO 24113 is overlaid onto the historical data; it can be seen that multiple solar cycles are encapsulated by this long-time duration.

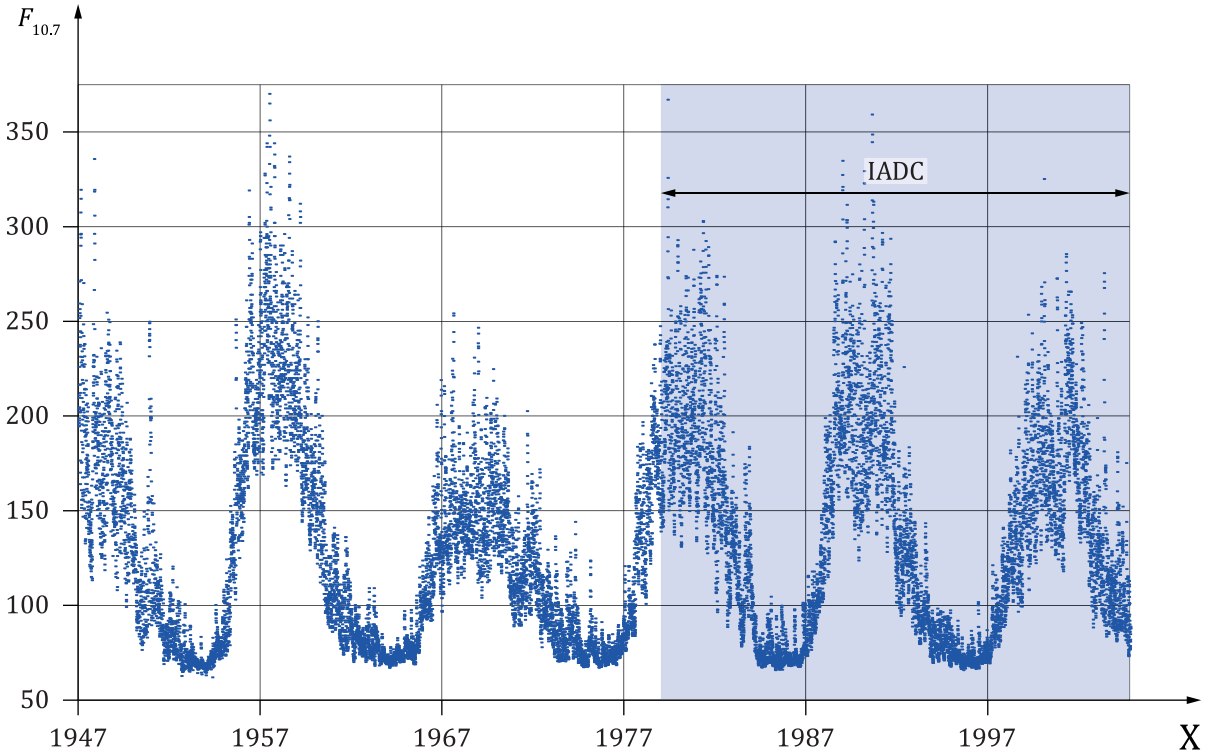

Key

X year

$F_{10.7}$ adjusted daily Ottawa/Penticton solar radio flux (at 10,7 cm wavelength)

Figure 2 — Solar cycle (≈11-year duration)

3.1.20
space debris
DEPRECATED: orbital debris
objects of human origin in *Earth orbit* (3.1.3) or re-entering the atmosphere, including fragments and elements thereof, that no longer serve a useful purpose

Note 1 to entry: *Spacecraft* (3.1.22) in reserve or standby modes awaiting possible reactivation are considered to serve a useful purpose.

3.1.21
space object
object of human origin which has reached outer space

3.1.22
spacecraft
system designed to perform a set of tasks or functions in outer space, excluding *launch vehicle* (3.1.8)

3.2 Symbols

a	orbit semi-major axis
A	spacecraft cross-sectional area with respect to the relative wind
A_p	Earth daily geomagnetic index
β	ballistic coefficient of spacecraft = $C_D * A / m$
C_D	spacecraft drag coefficient
C_R	spacecraft reflectivity coefficient
e	orbit eccentricity
$F_{10.7}$	solar radio flux observed daily at 2 800 MHz (10,7 cm) in solar flux units (10^{-22} W m^{-2} Hz^{-1})
$F_{10.7\ Bar}$	solar radio flux at 2 800 MHz (10,7 cm), averaged over three solar rotations
H_a	apogee altitude = $a\ (1 + e) - R_e$
H_p	perigee altitude = $a\ (1 - e) - R_e$
m	mass of spacecraft
R_e	equatorial radius of the Earth

3.3 Abbreviated terms

GEO	geosynchronous Earth orbit
GTO	geosynchronous transfer orbit
LEO	low Earth orbit
RAAN	orbit right ascension of the ascending node (angle between vernal equinox and orbit ascending node, measured counter-clockwise in equatorial plane, looking in the –Z direction of the chosen inertial frame)
SRP	solar radiation pressure

4 Orbit lifetime estimation

4.1 General requirements

The orbital lifetime of LEO-crossing mission-related objects shall be estimated using the processes specified in this document. In addition to any user-imposed constraints, the post-mission portion of the resulting orbit lifetime estimate shall then be constrained to a maximum of 25 years per ISO 24113 using a combination of:

a) initial orbit selection;

b) spacecraft vehicle design;

c) spacecraft launch and early orbit concepts of operation which minimize LEO-crossing objects;

d) spacecraft ballistic parameter modifications at end of life;

f) spacecraft deorbit manoeuvres.

4.2 Definition of orbit lifetime estimation process

The orbit lifetime estimation process is represented generically in Figure 3.

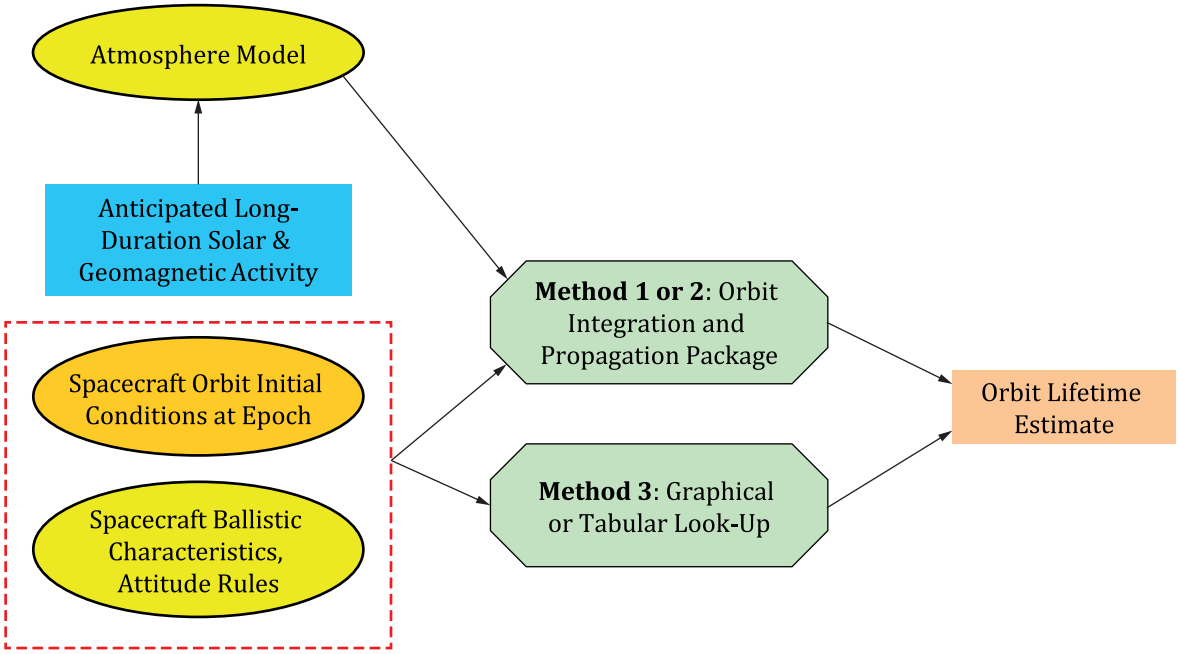

Figure 3 — Orbit lifetime estimation process[6]

5 Orbit lifetime estimation methods and applicability

5.1 General

There are three basic analysis methods used to perform a long-duration orbit lifetime prediction (ISO 24113), as depicted in Figure 1. Determination of the method used to estimate orbital lifetime for a specific space object shall be based upon the orbit type and perturbations experienced by the spacecraft as shown in Table 1.

Table 1 — Applicable method with mandated conservative margins of error (in per cent) and required perturbation modelling

	Special orbit:		Conservative margin applied to each method:			
Orbit apogee altitude (km)	**Sun sync?**	**High area-to-mass?**	**Method 1: numerical integration**	**Method 2: semi-analytic**	**Method 3: table look-up**	**Method 3: graph, equation fit**
Apogee < 2 000 km	No	No	Use β; no margin required	Use β; 5 % margin	Use β; 10 % margin	Use β; 25 % margin
Apogee < 2 000 km	No	Yes	Use β and SRP; no margin required	Use β and SRP; 5 % margin	Use β; 10 % margin	N/A
Apogee < 2 000 km	Yes	No	Use β; no margin required	Use β and SRP; 5 % margin	N/A	N/A
Apogee < 2 000 km	Yes	Yes	Use β and SRP; no margin required	Use β and SRP; 5 % margin	N/A	N/A
Apogee > 2 000 km	Either	Either	Use β and SRP and 3Bdy; no margin required	Use β and SRP and 3Bdy; 5 % margin	N/A	N/A

Key

N/A not applicable

β satellite ballistic coefficient

3Bdy third-body perturbations

SRP solar radiation pressure

Method 1, certainly the highest fidelity model, utilizes a numerical integrator with a detailed gravity model, third-body effects, solar radiation pressure, and a detailed spacecraft ballistic coefficient model. Method 2 utilizes a definition of mean orbital elements,[7] - [8] semi-analytic orbit theory and average spacecraft ballistic coefficient to permit the very rapid integration of the equations of motion, while still retaining reasonable accuracy. Method 3 is simply a table lookup, graphical analysis or evaluation of equations fit to pre-computed orbit lifetime estimation data obtained via the extensive and repetitive application of methods 1 or 2, or both.

5.2 Method 1: high-precision numerical integration

Method 1 is the direct numerical integration of all accelerations in Cartesian space, with the ability to incorporate a detailed gravity model (e.g. using a larger spherical harmonics model to address resonance effects), third-body effects, solar radiation pressure, vehicle attitude rules or aero-torque-driven attitude torques, and a detailed spacecraft ballistic coefficient model based on the variation of the angle-of-attack with respect to the relative wind. Atmospheric rotation at the Earth's rotational rate is also easily incorporated in this approach. The only negative aspects to such simulations are:

a) they run much slower than method 2;

b) many of the detailed data inputs required to make this method realize its full accuracy potential are simply unavailable;

c) any gains in orbit lifetime prediction accuracy are frequently overwhelmed by inherent inaccuracies of atmospheric modelling and associated inaccuracies of long-term solar activity predictions or estimates.

However, to analyse a few select cases where such detailed model inputs are known, this is undoubtedly the most accurate method. At a minimum, method 1 orbit lifetime estimations shall account for J_2 and J_3 perturbations and drag using an accepted atmosphere model and an averaged ballistic coefficient. In the case of high apogee orbits (e.g. GTO) or other resonant orbits, Sun and Moon third-body perturbations and solar radiation pressure effects shall also be modelled.

5.3 Method 2: rapid semi-analytical orbit propagation

Method 2 analysis tools utilize semi-analytic propagation of mean orbit elements [7] - [8] influenced by gravity zonals J_2 and J_3 and selected atmosphere models. The primary advantage of this approach over direct numerical integration of the equations of motion (method 1) is that long-duration orbit lifetime cases can be quickly analysed (e.g. 1 s versus 1 700 s CPU time for a 30-year orbit lifetime case). While incorporation

of an attitude-dependent ballistic coefficient is possible for this method, an average ballistic coefficient is typically used. At a minimum, method 2 orbit lifetime estimations shall account for J_2 and J_3 perturbations and drag using an accepted atmosphere model and an average ballistic coefficient. In the case of high apogee orbits (e.g. GTO), Sun and Moon third-body perturbations shall also be modelled.

5.4 Method 3: numerical table look-up, analysis and fit equation evaluations

In this final method, one uses tables, graphs and equations representing data that was generated by exhaustively using methods 1 and 2 (see 5.2 and 5.3). Graphs and equations provided in this document, along with other table lookup, analysis, and fit equations, can help the analyst crudely estimate orbit lifetime for their case of interest, permitting the analyst to estimate orbit lifetime for their particular case of interest via interpolation of method 1 or method 2 gridded data; all such method 3 data in this document were generated using method 2 approaches. At a minimum, method 3 orbit lifetime products shall be derived from method 1 or method 2 analysis products meeting the requirements. When using this method, the analyst shall impose at least a ten-percent margin of error to account for table look-up interpolation errors. When using graphs and equations, the analyst shall impose a 25 % margin of error.

5.5 Orbit lifetime sensitivity to Sun-synchronous orbit conditions

For Sun-synchronous orbits, orbit lifetime has some sensitivity to the initial value of RAAN due to the density variations with the local sun angle. Results from numerous orbit lifetime estimations show that orbits with 6:00 am local time have longer lifetime than orbits with 12:00 noon local time by about 5,5 %. [6] This maximum difference (500 days) translates into a 5 % error which can be corrected by knowing the local time of the orbit. As a result, method 1 or 2 analyses of the actual Sun-synchronous orbit condition shall be used when estimating the lifetime of Sun-synchronous orbits, with a 5 % error margin required for the semi-analytic approach.

5.6 Orbit lifetime statistical approach for high-eccentricity orbits (e.g. GTO)

For high-eccentricity orbits (particularly GTO), it can be difficult to iterate to lifetime threshold constraints due to the coupling in eccentricity between the third-body perturbations and the drag decay.[9],[10] Due to this convergence difficulty, only method 1 or 2 analyses shall be used when determining initial conditions which achieve a specified lifetime threshold for such orbits.

Sample analyses of GTO launcher stages [11]-[12] highlight this orbit lifetime sensitivity to initial conditions (orbit, spacecraft characteristic and force model), leading to a wide spectrum of orbital lifetimes.

Some theoretical considerations about the dynamical properties of GTO orbits are provided in References [11] and [13].

A test case illustrates the complex dynamical properties of GTO. Initial parameters are provided in Table 2.

Table 2 — GTO Initial Conditions for the Monte Carlo simulation

Perigee altitude	200 km
Apogee altitude	GEO altitude
Inclination	2°
Area to mass ratio	5e-3 m^2/kg
Solar activity	Constant ($F_{10.7}$=140 sfu A_p=15)
Drag coefficient	Constant = 2,2
Reflectivity coefficient	Constant = 2

Figure 4 shows lifetime results (years) when varying the initial date and the initial local time of perigee. This latest parameter is defined as the angle in the equator between the Sun direction and the orbit perigee, measured in hours. The date was chosen from day 1 to 365 in year 1998 and the local time of perigee was chosen by varying the right ascension of ascending node from 0 to 2π. A total of 2 500 different initial conditions were generated.

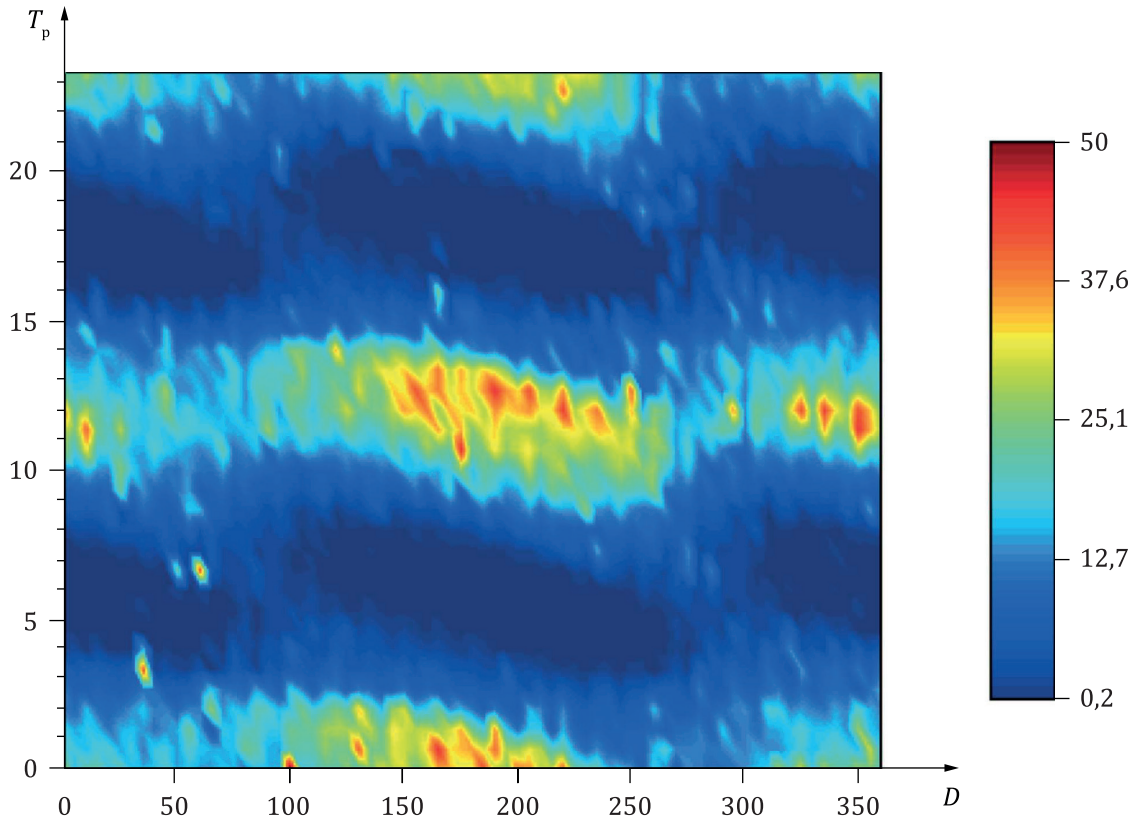

Key

D initial day of year, 1998

T_p initial local time of perigee passage, hours UTC

Figure 4 — Orbit lifetime as a function of initial day of year and local time of perigee

The shapes of the lifetime contours confirm that initial day of year and local time of perigee are initial conditions that make sense to describe GTO evolution since strong patterns are visible. The amplitudes of lifetimes variations are worth noting: from several months to more than 50 years. Previous results (see References [10] and [12]) are illustrated in Figure 4: the longest lifetimes are obtained for initial Sun-pointing (12 h local time) or anti Sun-pointing (24 h local time) perigee with an initial date around the solstices. The dark red pixels drawn in dark blue areas, as seen for initial day 60 and local time 7 h, are an indication of the presence of strong resonance phenomena. The year is also known to have an influence, to a lesser extent, through the Moon's perturbative effects.

Figure 5 shows semi-major axis evolution for several propagations of a typical low-inclined GTO. The different curves correspond to changes of 0,1 % or 1 % in the area to mass ratio of the object (A/m), which is far below the level of incertitude on this parameter. These dispersions lead to variations of decades in the re-entry duration. Such a strong non-linear behaviour is explained by the aforementioned resonances. One can see that semi-major axis evolutions are quite similar between all propagation cases until the entrance in the coupling between J_2 and Sun perturbations, for a semi-major axis equal to about 15 500 km. The duration of the resonance (period when the semi-major axis remains constant) and thus the rest of the propagation are completely different. A similar figure can be plotted by keeping the area to mass ratio constant and slightly changing the solar activity.

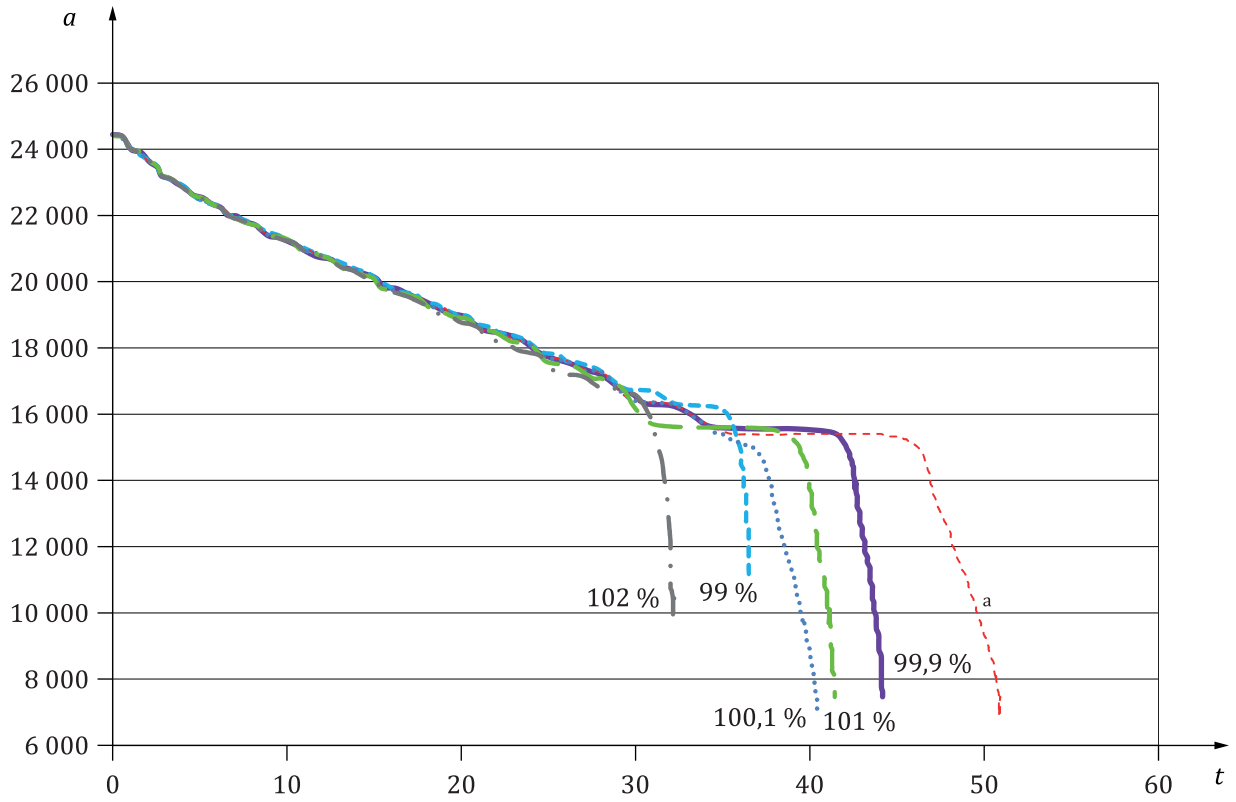

Key

t time, expressed in years

a semi-major axis, expressed in km

[a] Nominal A/m ratio (100 %).

Figure 5 — SMA evolution sensitivity to slight A/m variations (from 0,1 % to 2 %)

These examples show that resonance phenomena have substantial impacts on orbital elements evolution that can neither be predicted nor managed. Cumulated uncertainties on drag force between the extrapolation start (mission disposal manoeuvre for example) and the instant when the resonance occurs make the entry condition in this resonance prone to strong variations. As a consequence, trying to estimate lifetime of GTOs using only one extrapolation can lead to erroneous conclusion since tiny changes in the initial conditions, spacecraft characteristics or force models end in very different lifetime results. Exceptions to that would be objects on a GTO whose semi major axis has already decreased enough to avoid resonances or to be very close to them. However, since resonance conditions change with regards to the possible resonant angles, one can see that performing several propagation cases is advised to get robust results. As a conclusion, only statistical results are adequate to estimate the strong variations of GTO lifetimes.

As a consequence, one should not say “this object’s lifetime is Y years” in GTO but rather “the lifetime of this object is shorter than Y years with a probability p”, coming from a cumulative distribution function.

Key parameter uncertainties shall be taken into account in the lifetime estimation:

— initial conditions (date, orbit parameters);

— ballistic coefficient and drag coefficient;

— solar activity.

A Monte Carlo simulation test case [14] yields results that illustrate the variability in lifetime estimates. Initial parameters for this test case are described in Table 3. A total of 2 500 different initial conditions were generated.

Table 3 — Hypothesis conditions for the Monte Carlo simulation

Parameter	Nominal value	Dispersions
Perigee altitude	180 km	Small dispersions: 1 sigma standard deviation about 1 km, correlated to other orbit parameters
Apogee altitude	GEO altitude	Small dispersions: 1 sigma standard deviation about 50 km, correlated to other orbit parameters
Inclination	6°	Small dispersions: 1 sigma standard deviation about 0,01°, correlated to other orbit parameters
Area to mass ratio	5.e-3 m^2/kg	Uniform distribution ±20 % with respect to nominal value
Drag coefficient	Function of geodetic altitude	None
Reflectivity coefficient	Constant =1,5	None
Solar activity	Randomly chosen using data from the past	None
Date	Uniform distribution between day 1 and day 365, for years between 2015 and 2033	The dispersion of the year addresses Moon perturbations.
Local time of perigee	Gaussian distribution with a mean value of 22 h	Standard deviation of 50 min for time of perigee passage

Figure 6 and Figure 7 provide a statistical histogram and cumulative distribution function of orbit lifetime for this test case.

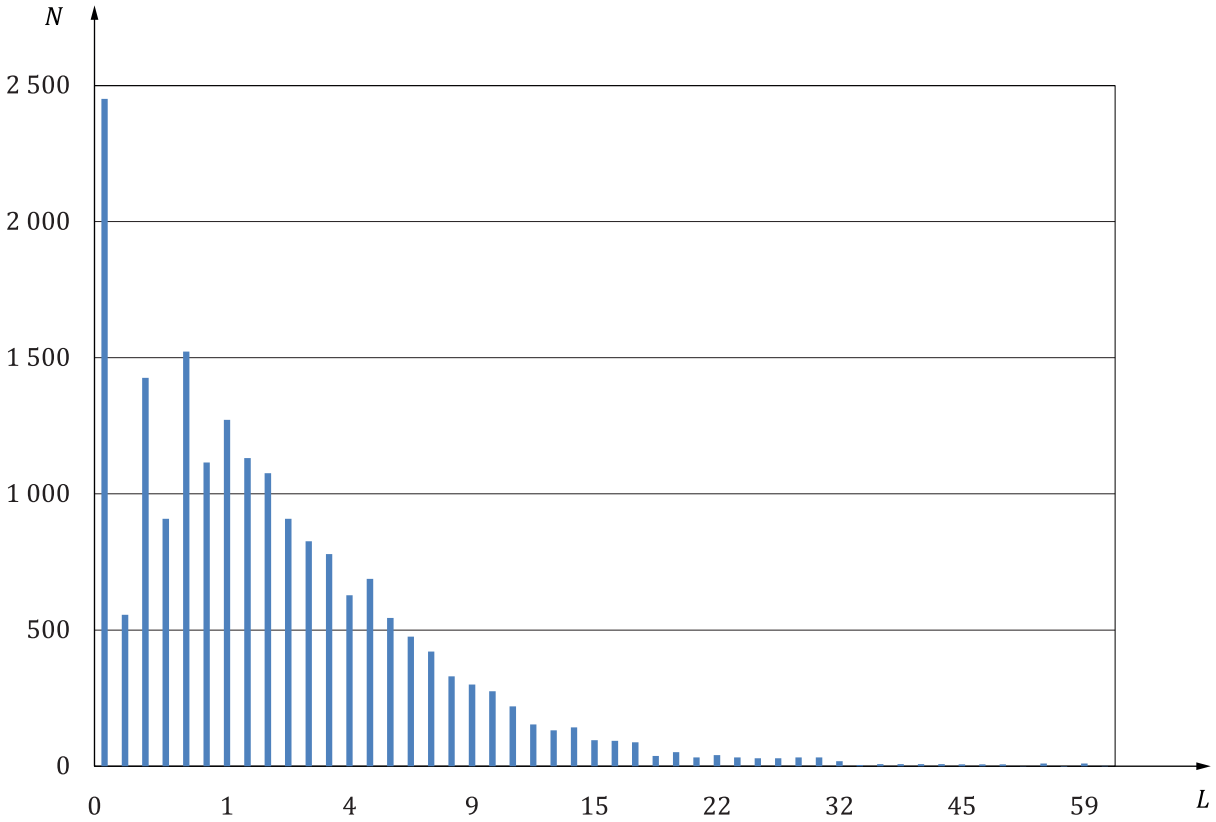

Key

L lifetime, expressed in years

N number of occurrences in this lifetime bin

Figure 6 — Histogram of orbital lifetimes

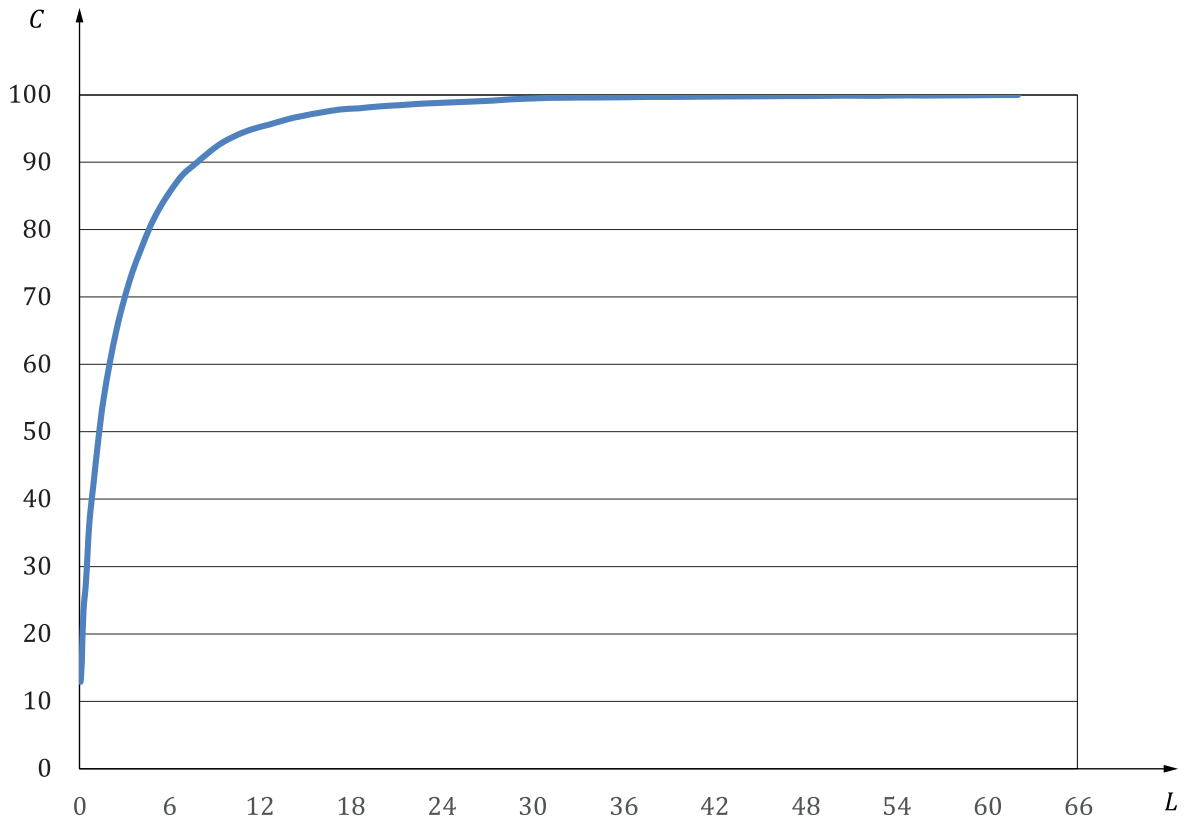

Key

L lifetime, expressed in years

C cumulative distribution function

Figure 7 — Cumulative distribution function of orbital lifetimes

The question of statistical convergence can be addressed by computing a confidence interval for the Monte Carlo results, associated to a confidence level. The so-called "interval of Wilson with correction for continuity" [15] has been well-adapted for this purpose.

In this approach, the upper p_1 and lower p_2 limits of this interval are given by Formulae (1) and (2):

$$p_1 = \frac{2nf + u_{\alpha/2}{}^2 - 1 - u_{\alpha/2}\sqrt{u_{\alpha/2}{}^2 - 2 - 1/n + 4f(n(1-f)+1)}}{2\left(n + u_{\alpha/2}{}^2\right)} \quad (1)$$

$$p_2 = \frac{2nf + u_{\alpha/2}{}^2 + 1 + u_{\alpha/2}\sqrt{u_{\alpha/2}{}^2 + 2 - 1/n + 4f(n(1-f)-1)}}{2\left(n + u_{\alpha/2}{}^2\right)} \quad (2)$$

Where

n	number of single runs (orbit propagations);
f	observed probability = number of lifetimes estimated to be lower than a certain value, divided by n;
$u_{\alpha/2} = \Phi^{-1}(1-\alpha/2)$	(= 1,96 for example for a confidence interval of 95 %). Φ is the cumulative normal distribution function.

As shown in Figure 8 and Figure 9, after N Monte Carlo runs one can compare the limit (upper or lower) of the confidence interval with the targeted probability for the lifetime to be lower than a certain value.

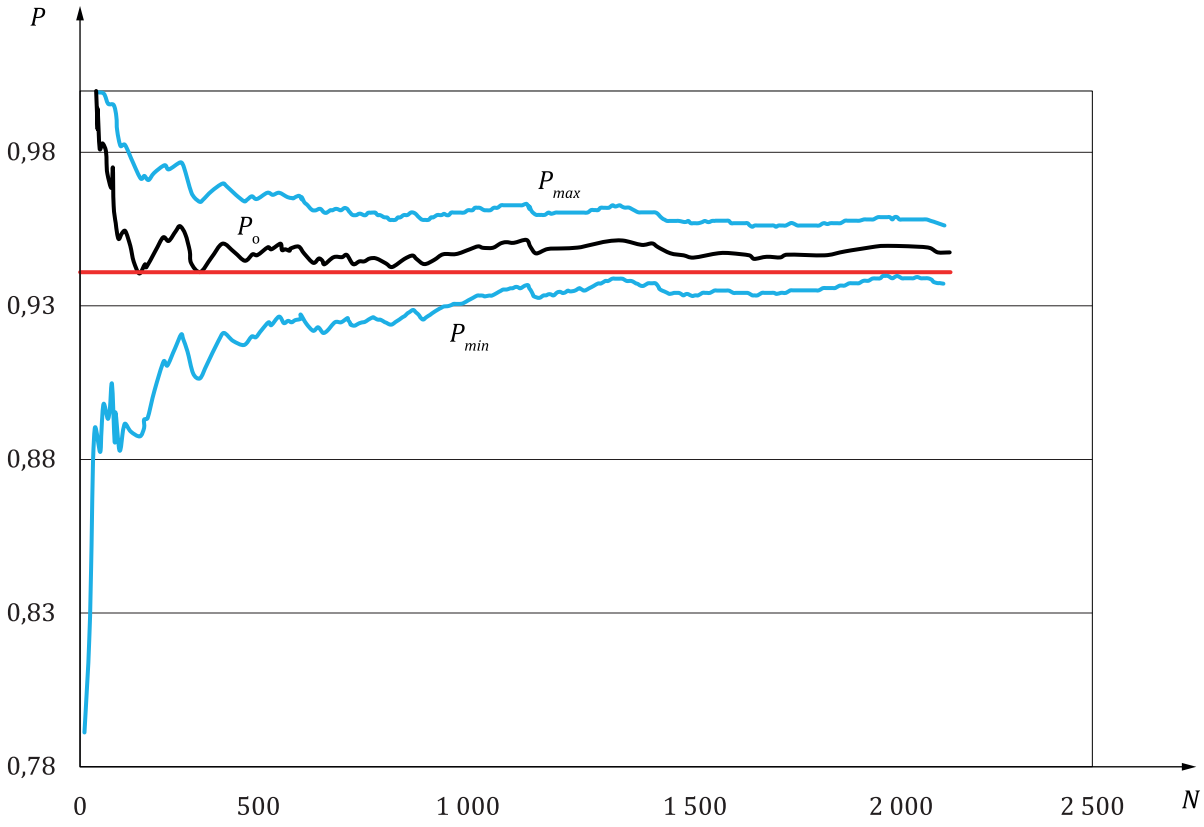

Key

N	number of simulations
P	probability
P_{max}	max probability of confidence interval
P_o	observed probability over N simulations
P_{min}	min probability of confidence interval

Figure 8 — Example of evolution of the observed probability (lifetimes lower than 25 years) and 95 % confidence interval

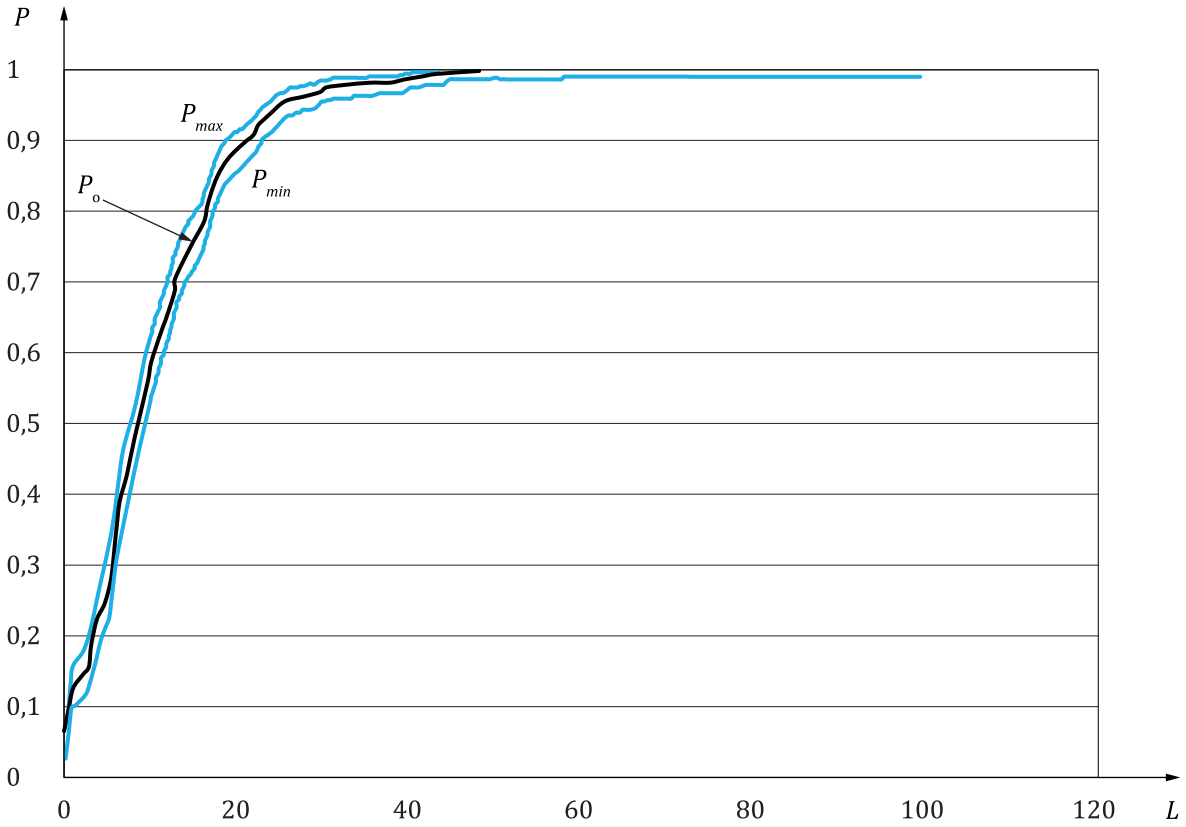

Key

L	lifetime, expressed in years
P	probability
P_{max}	max probability of confidence interval
P_o	observed probability over N simulations
P_{min}	min probability of confidence interval

Figure 9 — Example of cumulative distribution function of orbital lifetimes with a 95 % confidence interval (500 runs)

6 Atmospheric density modelling

6.1 General

The three biggest factors in orbit lifetime estimation are:

a) the selection of an appropriate atmosphere model to incorporate into the orbit acceleration formulation;

b) the selection of appropriate atmosphere model inputs;

c) determination of a space object's ballistic coefficient.

Each of these three aspects is examined.

6.2 Atmospheric drag models

There are a wide variety of atmosphere models available to the orbit analyst. The background, technical basis, utility, and functionality of these atmosphere models are described in detail in References [16] to [25]. This document does not presume to dictate which atmosphere model the analyst shall use. However, it is worth noting that in general, the heritage, expertise and especially the observational data that went into

creating each atmosphere model play a key role in that model's ability to predict atmospheric density, which is in turn a key factor in estimating orbit lifetime. Many of the early atmosphere models are of low fidelity and were originally created based on only one, or perhaps even just a part of one, solar cycle's worth of data.

The advantage of some of these early models is that they typically run much faster than the latest high-fidelity models (Table 4), without a significant loss of accuracy. However, the use of atmosphere models that were designed to fit a select altitude range (e.g. the "exponential" atmosphere model, "static" models, or models that do not accommodate solar activity variations) should be avoided in cases where they might miss too much of the atmospheric density variational complexity to be sufficiently accurate.

There are some early models (e.g. Jacchia 1971 of Table 4) which accommodate solar activity variations and also run very fast; these models can work well for long-duration orbit lifetime studies where numerous cases are to be examined. Conversely, use of the more recent atmosphere models are encouraged because they have substantially more atmospheric drag data incorporated as the foundation of their underlying assumptions. A crude comparison of a sampling of atmosphere models for a single test case is shown in Figure 10 and Figure 11, illustrating the range of temperatures and densities exhibited by the various models. ISO 14222 provides guidance on a variety of suitable atmosphere models and associated indices. Although this document does not presume to direct which atmosphere model the analyst should use, the lengthy prediction timespan associated with this document makes several of the atmosphere models listed in ISO 14222 suitable for estimation of orbital lifetimes spanning 25 years or more, to include, but not limited to, the NRLMSISE-00,[20] NRL MSIS Version 2,[27] JB2006,[21] JB2008,[22] GRAM-07,[23] DTM-2000 [24] and GOST [25] models.

Table 4 — Comparison of normalized density evaluation runtimes

Atmosphere model	0 < Alt < 5 000 km	0 < Alt < 1 000 km
Exponential	1,00	1,00
Standard Atmosphere 1962	1,43	1,51
Standard Atmosphere 1976	1,54	1,54
Jacchia 1971	13,68	17,31
MSIS 2000	141,08	222,81
JB2006	683,85	584,47

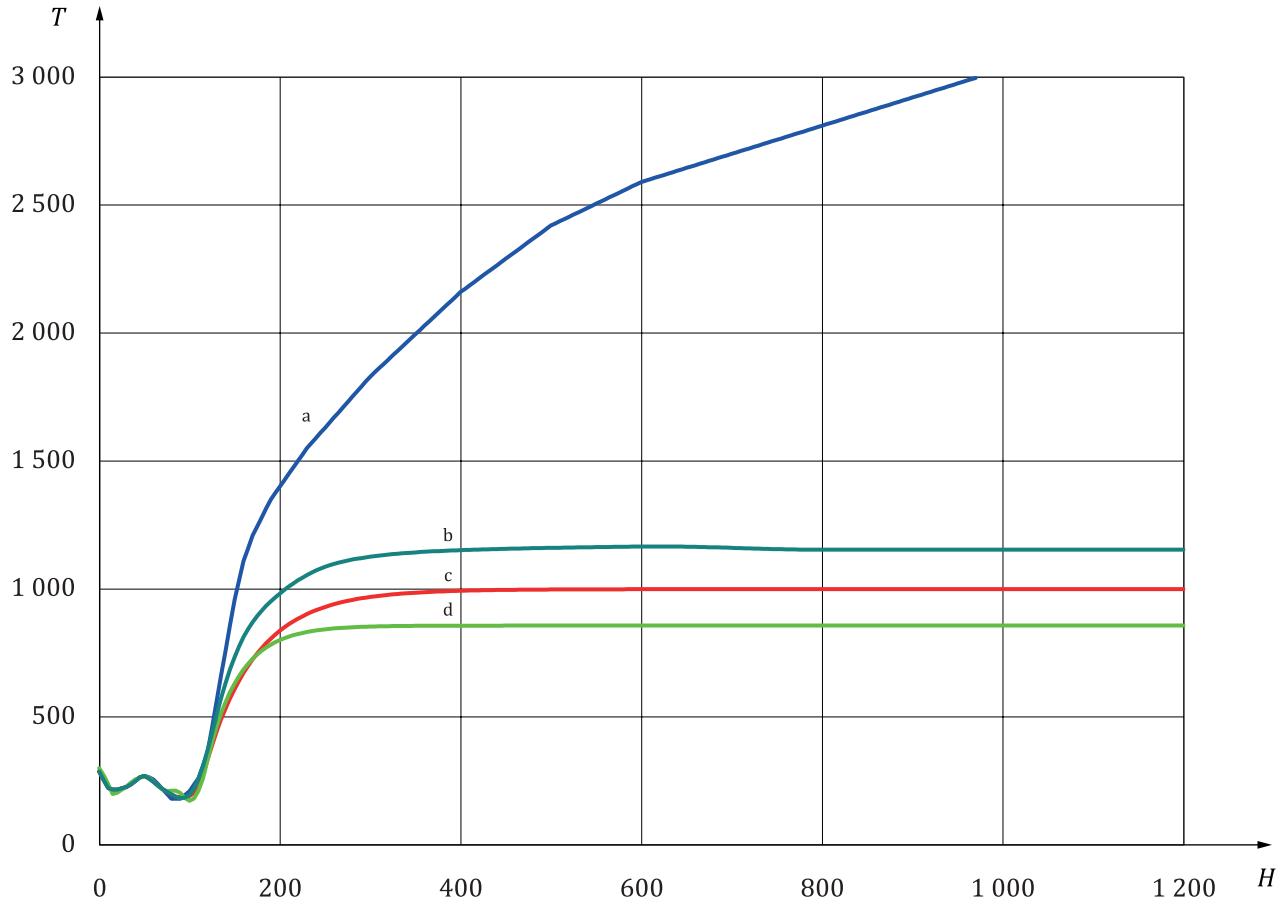

Key

H altitude, expressed in km

T temperature, expressed in K

a 1962 std atmosphere model.

b 2006 Jacchia-Bowman atmosphere model.

c 1976 std atmosphere model.

d 2000 MSIS atmosphere model.

Figure 10 — Temperature comparison by atmosphere model

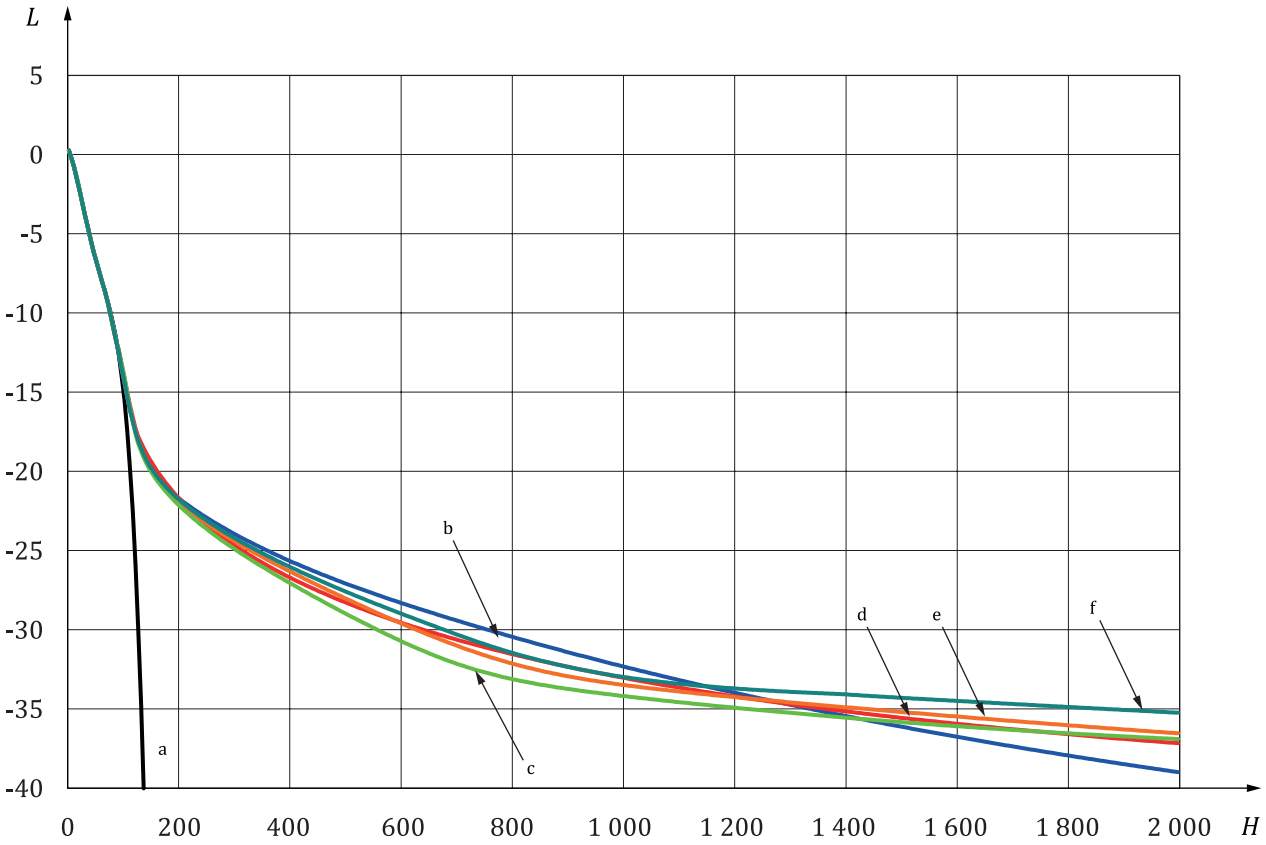

Key

H altitude, expressed in km

L log10(density in kg/m^3)

a Exponential model.

b 1962 std atmos.

c MSIS E 2000.

d Jacchia 1976.

e Jacchia 1971.

f JB2006.

Figure 11 — Comparison of a small sampling of atmosphere models

6.3 Long-duration solar flux and geomagnetic indices prediction

Utilization of the higher-fidelity atmosphere models mentioned in 6.2 requires the orbit analyst to specify the solar and geomagnetic indices required by such models. Compatible input indices are needed for each model; subtle difference can exist in the interpretation of similarly named indices when used by different atmosphere models (e.g. centrally averaged vs. backward averaged $F_{10.7\ \mathrm{Bar}}$).

Key issues associated with any prediction of solar and geomagnetic index modelling approach are as follows.

a) $F_{10.7\ \mathrm{Bar}}$ predictions should reflect the estimated mean solar cycle as accurately as possible. One such prediction is shown in Figure 12.

b) Large daily $F_{10.7}$ and A_p index variations about the mean value induce non-linear variations in atmospheric density, and the selected prediction approach should account for this fact; i.e. one should account for the highly non-linear aspects of solar storms versus quiet periods.

c) The frequency of occurrence across the day-to-day index values is highest near the lowest prediction boundary (Figure 13).

d) $F_{10.7}$ cycle timing/phase are always imprecise and should be accounted for; the resultant time bias that such a prediction error would introduce can yield large $F_{10.7}$ prediction errors of 100 % or more.

e) The long-time duration orbit lifetime constraint specified in ISO 24113 (i.e. 25 years) would require that the solar/geomagnetic modelling approach provide at least that many years (i.e. 25) of predictive capability.

f) Predicted $F_{10.7}$ values should be adjusted to correct for Earth-Sun distance variations.

g) Some atmosphere models (e.g. JB2006 and JB2008), due to the newly invented indices adopted thereby, preclude the use of historical indices for long-term orbit lifetime studies, while currently also precluding use of any predictive forecasting model(s) for those indices until such time as those become publicly available.

Accounting for these constraints, the user shall adopt one of the four acceptable approaches.

— Space weather approach #1: Utilize Monte Carlo sampling of historical data [28],[29] mapped to a common solar cycle period.

— Space weather approach #2: Utilize a predicted $F_{10.7\ Bar}$ solar activity prediction profile generated by a model such as is detailed in Figure 12,[24] coupled with a stochastic or similar generation of corresponding $F_{10.7}$ and A_p values (e.g. see Reference [30]).

— Space weather approach #3: Utilize a "mean equivalent static" set of solar and geomagnetic activity. While such an approach produces equivalent solar and geomagnetic indices that are suitable for efficient and equivalent orbit lifetime estimation, such static values are only valid for the cycles fit, the selected orbit prediction span (i.e. 25 years) with an associated probability level and the adopted atmosphere model. New sets of mean equivalent static indices would likely need to be generated for any changes in these functional dependencies.

— Space weather approach #4: Utilize the recommended solar forcing dataset for the Coupled Model Intercomparison Project 6 through which the atmospheric modelling community assesses future climate change.

Since approach #2 is a well-known and common approach, the focus of this clause is on the Monte Carlo "random draw" approach (ISO 24113) (approach #1), the "mean equivalent static" approach[15,31-35] (approach #3), and the solar forcing dataset for the Coupled Model Intercomparison Project 6 (approach #4).

6.4 Method 1: Monte Carlo random draw of solar flux and geomagnetic indices

More than six solar cycles of observed solar and geomagnetic data exist to choose from (Figure 2). Processing of this data maps each coupled and correlated triad of datum ($F_{10.7}$, $F_{10.7\ Bar}$, and A_p) into a single solar cycle range of 10,825 46 years (3 954 days), with the 'averaged' solar minimum referenced to 25 February 2007.

By mapping this historical data into a single solar cycle (Figure 14, Figure 15, and Figure 16), the user can then sample coupled triads of ($F_{10.7}$, $F_{10.7\ Bar}$, and A_p) data corresponding to the orbit lifetime simulation day within the mapped single solar cycle as discussed in Annex B. This solar/geomagnetic data can then be updated at a user-selectable frequency (e.g. once per orbit or day), thereby simulating the drag effect resulting from solar and geomagnetic variations consistent with historical trends for these data. Since daily data has been accumulated since February 14, 1947, on any given day within the 3 954-day solar cycle at least five data triads exist to choose from. To preserve any statistical interdependencies (particularly between $F_{10.7}$ and $F_{10.7\ Bar}$), it is important that the random draw retain the integrity of each data triad, since $F_{10.7}$, $F_{10.7\ Bar}$ and A_p are interrelated.

In the Monte Carlo approach for modelling solar and geomagnetic data, coupled triads of ($F_{10.7}$, $F_{10.7\ Bar}$, and A_p) data are selected for each day (or alternately for each orbit rev) of the orbit lifetime simulation, thereby simulating the drag effect resulting from solar and geomagnetic variations consistent with historical trends for these data. The atmospheric density estimated from atmospheric models utilizing a given ($F_{10.7}$, $F_{10.7\ Bar}$, and A_p) triad can then be directly utilized by either method 1 (numerical integration) or method 2 (semi-analytic) approaches. Due to the introduced step-function change in atmospheric density, it can be beneficial to restart method 1 integration at each parameter set change; for semi-analytic (e.g. with orbital revolution

time steps via Gaussian quadrature), a new parameter set can be drawn at an orbit revolution time step; thus, no numerical difficulties will be introduced.

If known, the starting epoch of the simulation shall be selected to match the anticipated actual end-of-mission epoch. Alternately, starting epochs may be sampled throughout the entire aggregate solar cycle and to ensure that the median (50th-percentile) value meets the specified orbit lifetime criteria of ISO 24113.

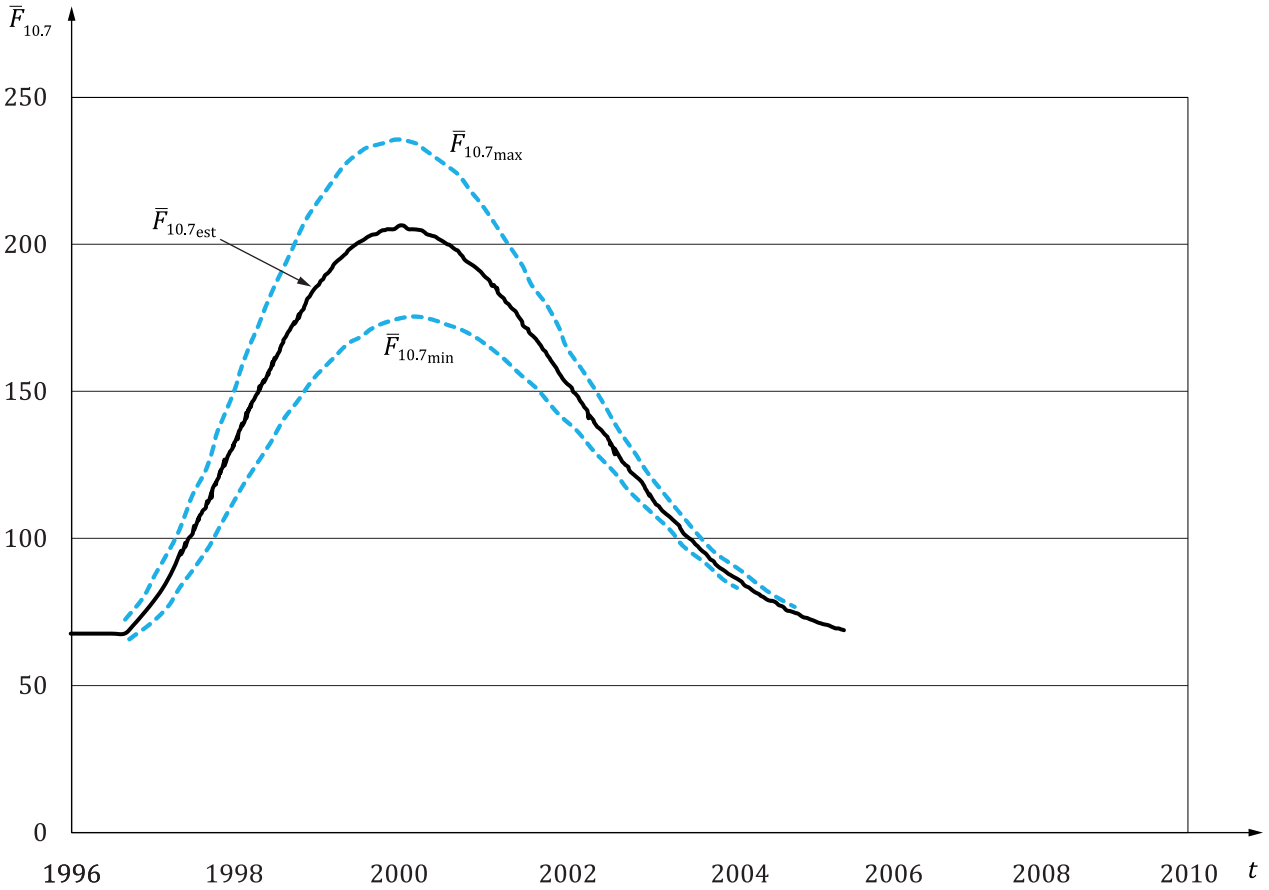

Key

t	time, expressed in years
$\bar{F}_{10.7}$	81-day average solar flux at 10,7 cm
$\bar{F}_{10.7_{max}}$	max probability of confidence interval
$\bar{F}_{10.7_{est}}$	observed probability over N simulations
$\bar{F}_{10.7_{min}}$	min probability of confidence interval

Figure 12 — Solar flux estimated upper, lower and representative trends

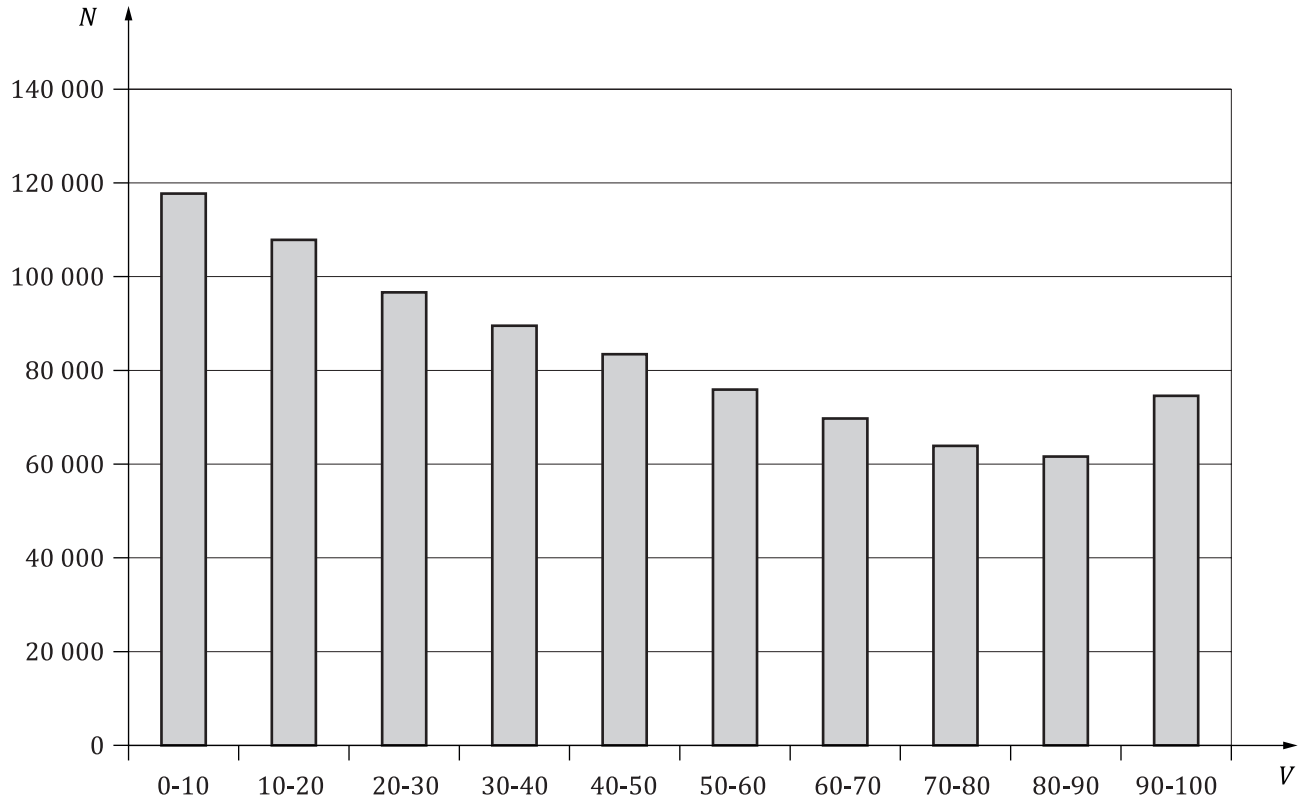

Key

V variability, expressed as the percentage ranging from 0 % (minimum value) to 100 % (maximum value)

N number of daily occurrences between 1947 and 2006

Figure 13 — Distribution of $F_{10.7}$ daily percentile values within monthly minimum/maximum $F_{10.7}$ range

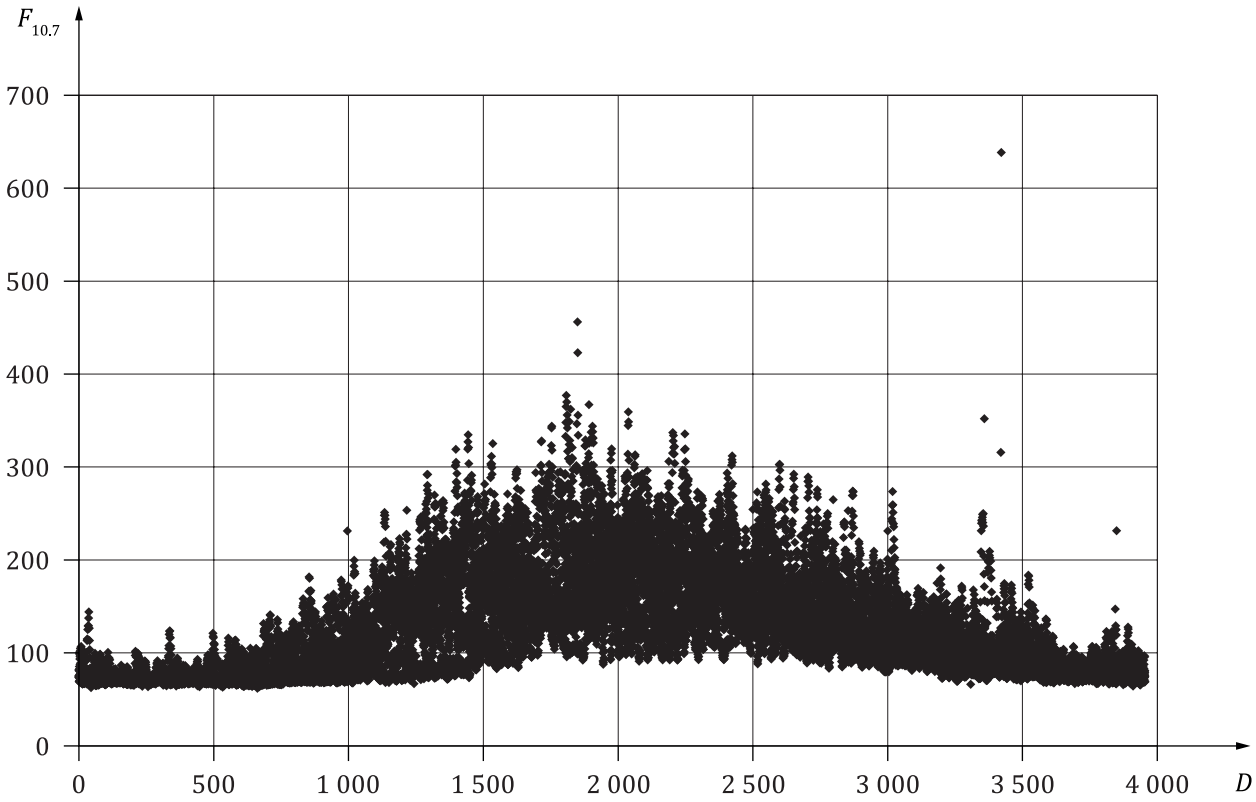

Key

D days from start of normalized solar cycle

$F_{10.7}$ solar flux at 10,7 cm modulo to one solar cycle timespan of average length

Figure 14 — $F_{10.7}$ normalized to average solar cycle

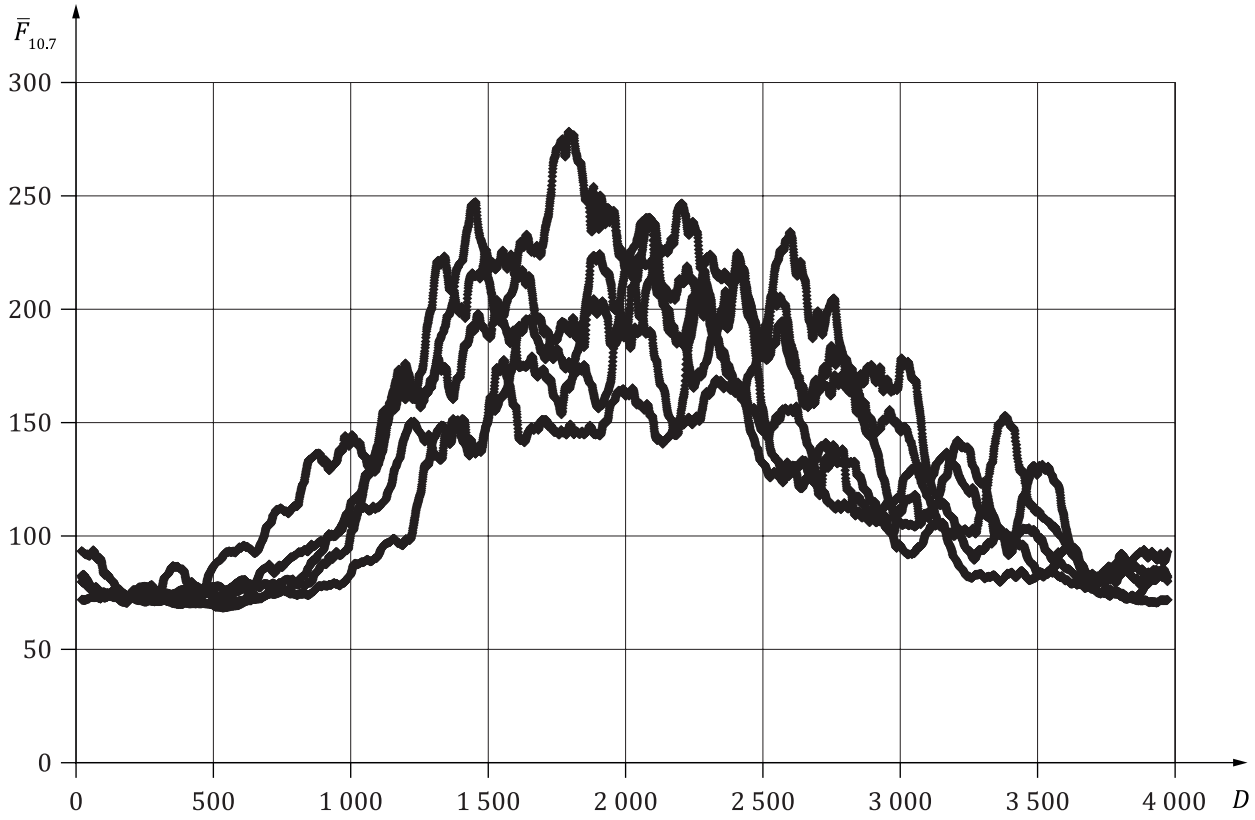

Key

D days from start of normalized solar cycle

$\bar{F}_{10.7}$ solar flux index averaged over 3 solar rotations ~ 81 days), modulo to one solar cycle timespan of average length

Figure 15 — $F_{10.7\ \mathrm{Bar}}$ normalized to average cycle

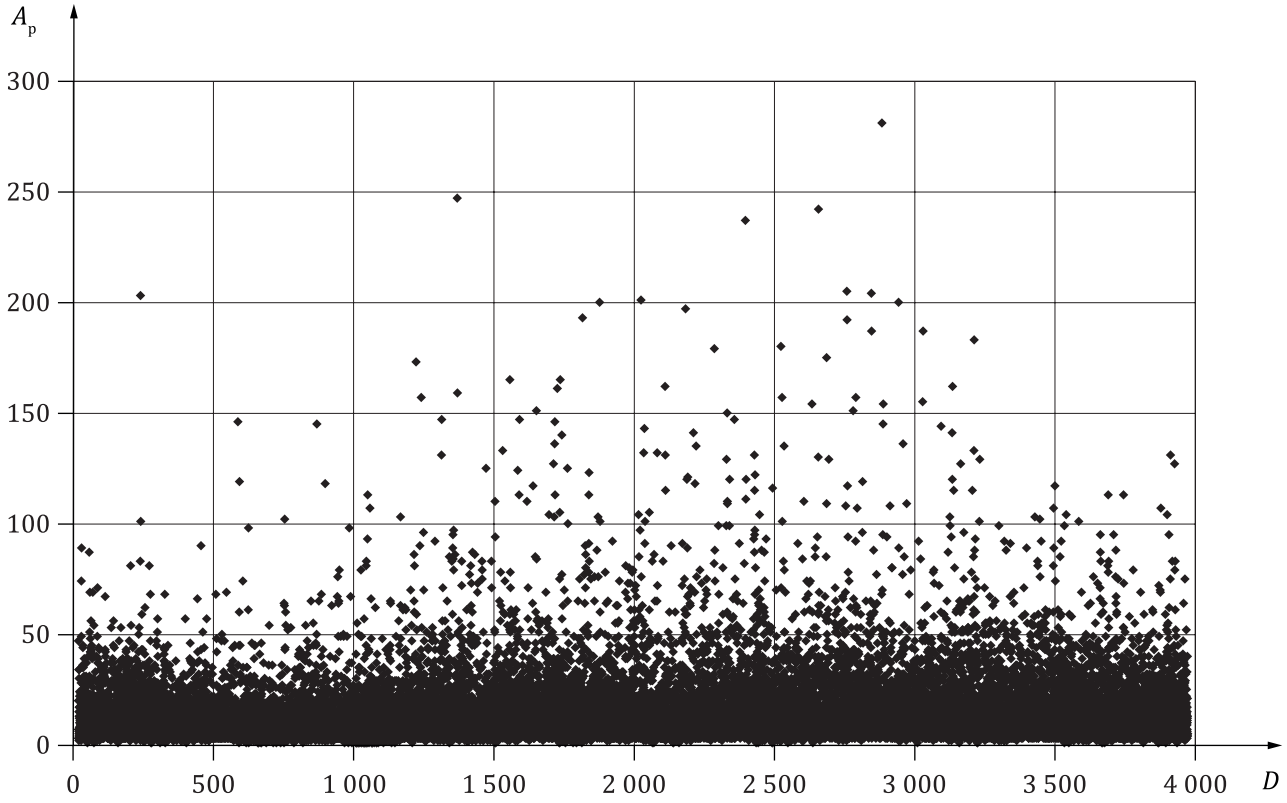

Key

D days from start of normalized solar cycle

A_p geomagnetic flux modulo to one solar cycle timespan of average length

Figure 16 — A_p normalized to average cycle

It can be seen from Figure 16 that A_p is:

a) unpredictable;

b) loosely correlated with the solar cycle;

c) volatile.

Figure 17 demonstrates that density varies greatly (i.e. several orders of magnitude) depending upon A_p; thus, a geomagnetic storm can induce large decreases in orbital energy (orbit decay) that the use of some average A_p value would miss. Correspondingly, the analyst should incorporate A_p variations into the geomagnetic index predictions.

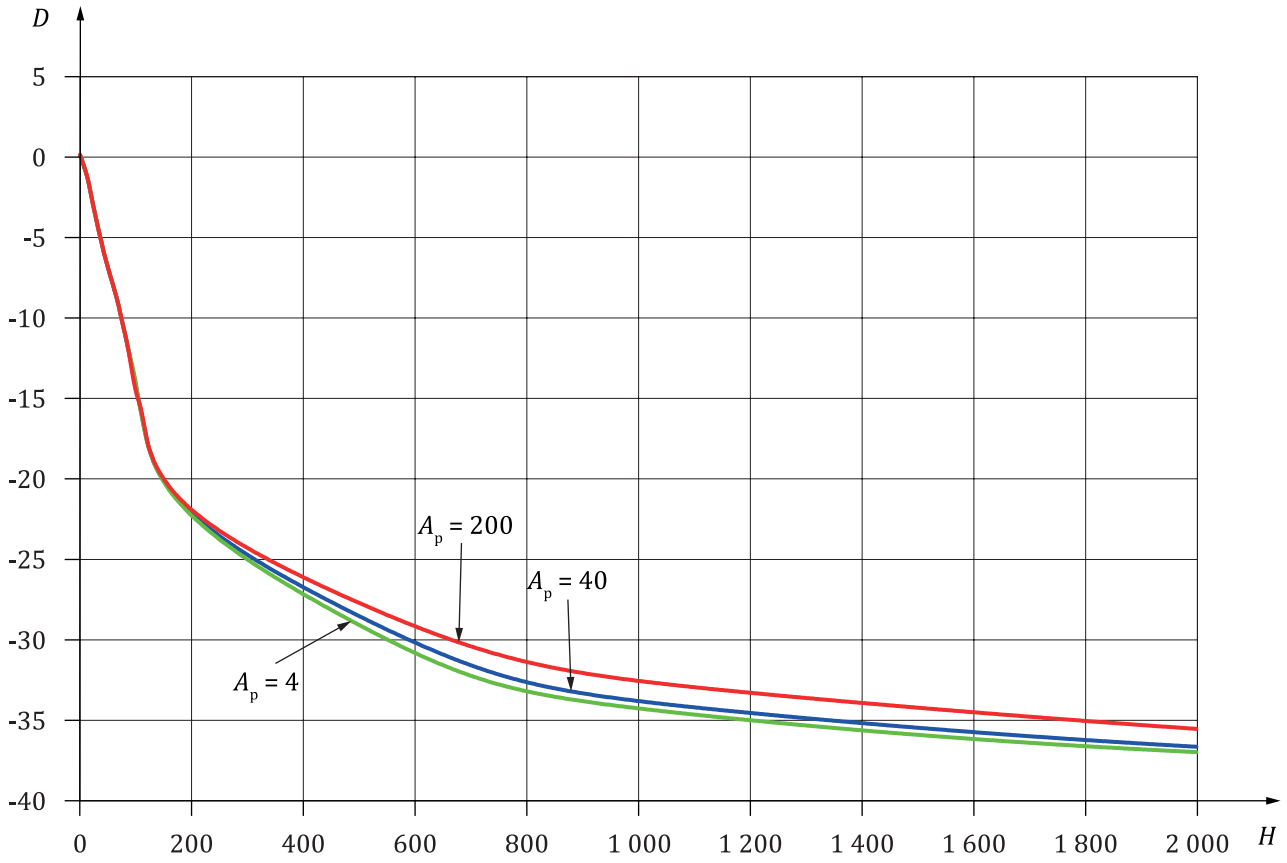

Key

H altitude, expressed as km above oblate spheroid

D Log10(density in square cm per kg)

Figure 17 — Log(density) variation as a function of altitude and A_p value

6.5 Method 2: predicted $F_{10.7\ Bar}$ solar activity prediction profile

The second approach for simulation of solar flux and geomagnetic indices is the use of long-term predictions as is discussed in 6.4 and shown in Figure 12.

6.6 Method 3: equivalent constant solar flux and geomagnetic indices

A third method for simulation of solar flux and geomagnetic indices is the use of "equivalent constant solar flux and geomagnetic indices". In this method, the user generates (or obtains from a qualified third party) and incorporates precomputed constant equivalent values of solar flux and geomagnetic activity into the orbit lifetime estimation process which will yield the same orbital lifetime as would the use of actual measured (dynamic) indices. Since the starting epoch with respect to solar cycles is sometimes not well known and is a sensitive parameter of orbit lifetime estimation (about ±4 years for a typical LEO orbit), the starting epoch can be included in the Monte Carlo as a random parameter (the initial day is a random realization within the first solar cycle). This pre-computation of equivalent constant indices avoids the use of random draws each orbit and repeated Monte Carlos for the actual orbit of interest.

The equivalent constant indices shall be carefully tuned for any atmosphere model and orbit inclination of interest by the analyst. Use of tuned indices shall be verified to match historical solar and geomagnetic influences on orbit decay over a long-duration (i.e. 25-year) timespan and for the orbit inclination of interest. This ensures that a space object having a specific ballistic coefficient and starting orbit that has a 25-year lifetime computed by using the constant equivalent solar activity yields an orbit lifetime estimate of less than 25 years with a *z* % probability level (see Figure 18).

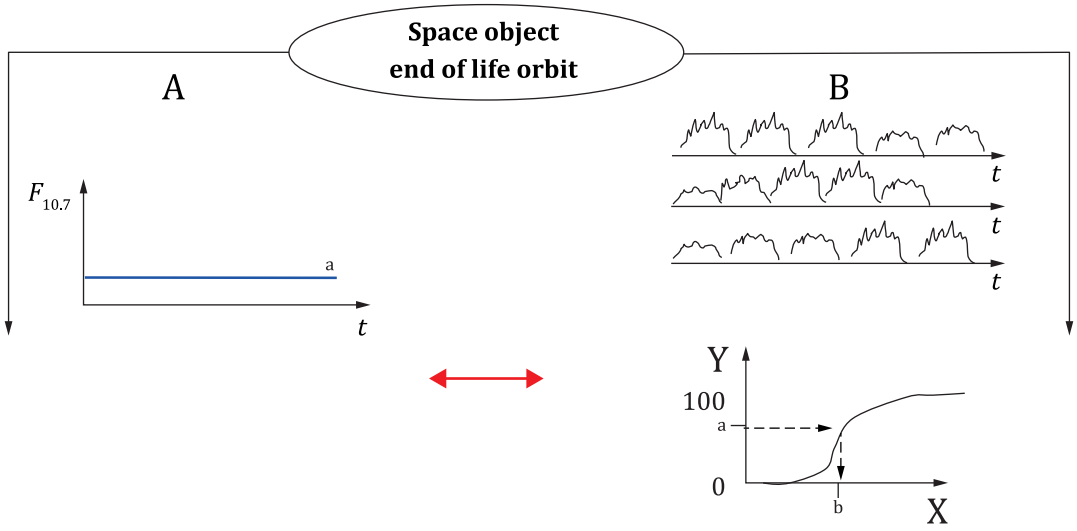

Key

X lifetime

Y lifetime adhering to constraint in z % of all cases

t orbit lifetime constraint duration

A equivalent constant solar activity

B possible future solar activities

a z %.

b Constraint.

Figure 18 — Statistical equivalency between constant and variable solar activity

Equivalent constant solar flux and geomagnetic activity indices are obtained via the following steps.

a) Select the initial orbit and a ballistic coefficient.

b) Select a representative geomagnetic A_p index (e.g. 15).

NOTE As there are two uncertain parameters (solar flux and geomagnetic index) with no evident correlation between them, this method is faced with two degrees of freedom versus only one output (estimated orbit lifetime). The method circumvents this by adopting a representative geomagnetic A_p index value which is averaged over the timespan of interest (e.g. 25 years) or more.

c) Using the random draw Monte Carlo approach previously outlined (method #1), generate n possible future solar activities (including random draws of starting date which encompass all possible launch dates, including launch slips).

d) Estimate orbit lifetime using the solar activity profiles, where n is appropriately sized using Dagum (Chernoff – Hoeffding) bounding methods.

e) As shown in Figure 19 and adopting z % to be 50 % (the median value), determine O_m (the median orbit lifetime of the trials).

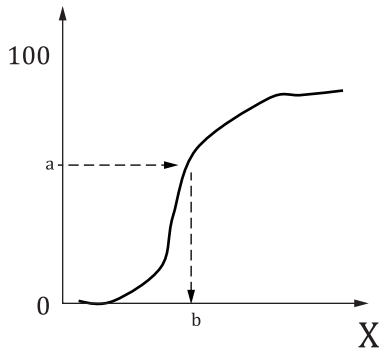

Key

X life time

a z %.

b OLT_7 %.

Figure 19 — Lifetime cumulative distribution function

f) Iterate on either initial orbit semi-major axis or perigee altitude until an $O_{50\ \%}$ of 25 years is found. At every step estimate n orbit lifetimes using new (randomly-drawn) solar activity profiles. The orbit that has an $O_{50\ \%}$ of 25 years is called the end-of-life limiting orbit.

g) Using the solved-for end-of-life limiting orbit, determine by iteration the constant equivalent solar flux index ($F_{10.7\_50\ \%}$ as shown in Figure 20) which also yields an orbit lifetime of 25 years.

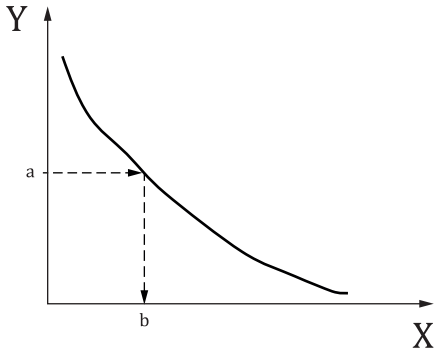

Key

X constant $F_{10.7}$

Y lifetime

a Lifetime constraint.

b $F_{10.7\_z\ \%}$.

Figure 20 — $F_{10.7\_z\%}$ value computation

h) Determine the viability region of the solved-for $F_{10.7\_z\%}$ value as a function of:

1) initial orbit inclination;

2) orbit eccentricity;

3) ballistic coefficient of the space object;

4) local time of the ascending node;

5) atmosphere model.

i) It is the task of the analyst to ensure that the equivalent constant solar activity values or expressions derived through these steps are applicable to the end-of-mission orbits to be analysed.

j) Parametric runs can be used to yield functional relationships for constant equivalent solar flux as a function of ballistic coefficient, orbit altitude(s), inclination, etc. One such expression for constant equivalent ("mean equivalent static") solar activity has defined as follows [33]:

$$A_p = 15 \tag{3}$$

$$F_{10.7} = 201 + 3{,}25 \ln(\beta) - 7 \ln(Z_a) \tag{4}$$

β is the ballistic coefficient, which equals $C_D * A / m$ (m^2/kg);

Z_a is the apogee radius (mean parameter) minus Earth radius (6 378 km), Z_a < 2 200 km.

For extrapolation using a variable drag coefficient vs altitude, a constant value of C_D shall be used to compute the constant equivalent solar activity. A C_D value of 2,2 has been chosen, but the analyst is encouraged to select a more appropriate value if warranted.

Figure 21 shows a plot of $F_{10.7}$ values using the parametric Formula (4) for several ballistic coefficients and apogee altitudes.

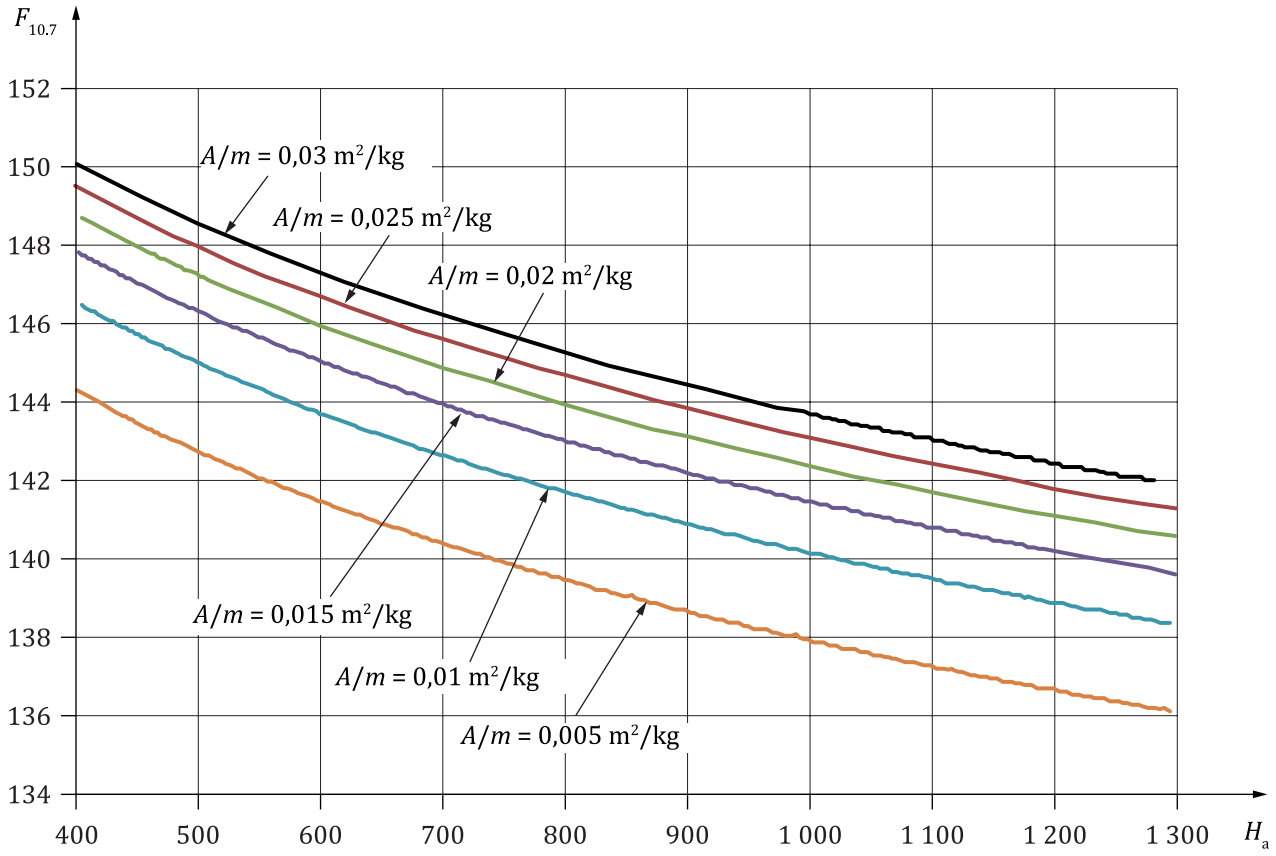

Key

H_a apoapsis altitude, expressed in

$F_{10.7}$ constant equivalent flux values

Figure 21 — Constant equivalent flux values (drag coefficient of 2,2 assumed)

If done correctly, the Monte Carlo approach #1 (random draws of initial date and solar activity) and approach #3 (equivalent constant solar flux index) should yield the same orbit lifetime.

Figure 22 depicts a typical LEO cumulative distribution function of lifetimes considering random initial date and solar activity (Monte Carlo). The perigee has been tuned to obtain p = 0,5 for 25 years. The same 25 years lifetime is obtained with one run considering the constant equivalent solar activity.

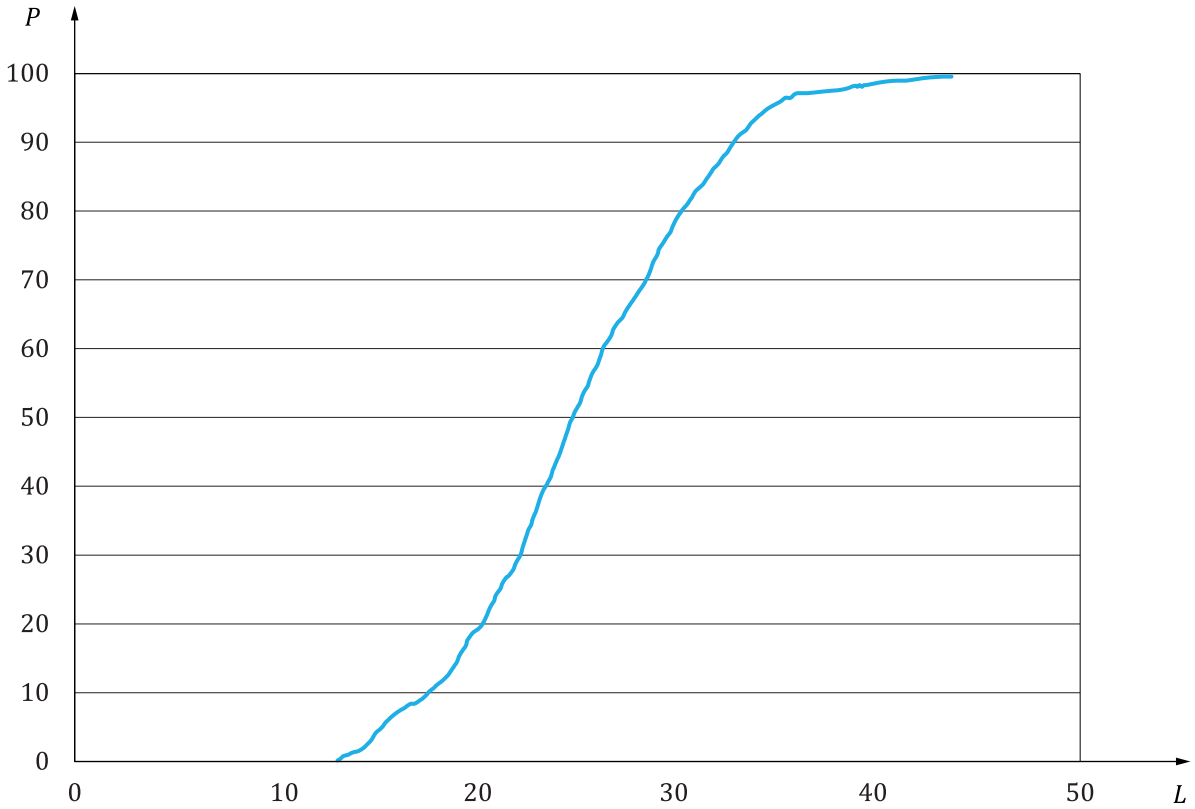

Key

L lifetime, expressed in years

P percent of cumulative density function

Figure 22 — Typical LEO cumulative distribution function considering random initial date and solar activity

6.7 Method 4: reference solar forcing scenario

A fourth method for simulation of solar flux and geomagnetic indices is the use of the recommended solar forcing dataset for the Coupled Model Intercomparison Project 6 through which the atmospheric modelling community assesses future climate change. This dataset[36] provides the $F_{10.7}$, A_p and K_p indices until the year 2300 (more detailed information on solar radiative and particle forcings is also supplied but is not needed for the relatively simple atmospheric models that are typically used for orbit lifetime estimation). The full dataset is available[37].

7 Atmospheric density implications of thermospheric global cooling

Recent indications of global cooling in the thermosphere can affect orbit lifetime estimations. The thermosphere is defined to occur roughly between 80 km and 500 km altitude, which is a key part of the LEO regime for which this document is applicable. Both spacecraft measurements and theoretical models indicate that the thermosphere is cooling off[25],[38],[39],[40] causing density to lower. The entire middle and upper atmosphere conditions have experienced cooling and contraction, resulting in a decline in thermosphere density at fixed heights. It is estimated that because of this effect, atmospheric density has

decreased by between 1,7 % and 2 % [39],[40] per decade. This decrease yields a corresponding increase in orbit lifetime of between 4 % and 7 %[6].

Such thermospheric density decreases are estimated to only increase with time. With CO_2 concentrations likely to increase more rapidly in the future, the reduction in thermosphere density is also expected to speed up. Reference [41] noted that under a moderate CO_2 forcing scenario, the future thermosphere density trend (2015-2070) is expected to approximately double compared to the historical period.

Scaling coefficients that can be used in conjunction with empirical models such as NRLMSIS 2.0 to take into account the effect of future reductions in thermosphere density associated with CO_2-induced cooling and contraction are provided in Reference [42]. They also estimated the impact of future density reductions for several example objects. They concluded that by 2030, a 27 % to 30 % reduction in thermosphere density at 400 km altitude compared to the year 2000 is likely, which would also increase orbital lifetimes by about 30 %.

8 Estimating ballistic coefficient (β)

8.1 General

The first step in planning a LEO-crossing space object disposal is to estimate the ballistic coefficient. Accurate estimation of the space object's ballistic coefficient is another key element in the orbit lifetime analysis process. Frequently, the analyst will select an average ballistic coefficient for the duration of the prediction, but this is not always the case. Cross-sectional area and drag coefficient estimations are now examined separately. Spacecraft mass shall be varied according to best-available knowledge but can typically be assumed to be constant from end of life until orbit decay.

8.2 Estimating aerodynamic force and solar radiation pressure coefficients

8.2.1 General

Drag, along with solar radiation pressure and third body effects as discussed in Annex C, can influence orbit lifetime.

A reasonable value of the dimensionless drag coefficient, C_D, is 2,2 for a typical spacecraft. However, the drag coefficient, C_D, depends on the shape of the spacecraft and the way air molecules collide with it. For certain geometric configurations such as spheres, cylinders and cones, the value of axial drag coefficient, C_D, can be evaluated more precisely than previously noted provided something is known about the flow regime and reference area. The analyst shall consider C_D variations based on spacecraft shape and anticipated uncontrolled attitudinal stability. The drag coefficient can become considerably higher than 2,2 for elongated spacecraft shapes; for those shapes, a more accurate result can be obtained by using the "panel model" described in 8.2.2.

C_D is known to vary as a function of attitude (for asymmetric objects) and orbit altitude. But for long-duration orbit lifetime estimations, these effects can potentially be ignored or averaged out since the orbit lifetime percent error can be quite small due to averaging effects over very long-duration (e.g. 25 year) orbit lifetime time spans.

8.2.2 Aerodynamic and solar radiation pressure coefficient estimation via a "panel model"

If the spacecraft shape is not overly complex, aerodynamic force and SRP coefficients can be estimated using a spacecraft panel model.[43],[44],[45] A panel model consists in its simplest form of a set of $i = 1, \ldots, N$ panels, each panel described only by its area A_i and its outward normal unit vector $\hat{n}_i$ that defines its orientation in a spacecraft body-fixed frame with respect to the relative wind as shown in Figure 23.

These models do not provide information on the shape and relative position of each panel. Obscuration of one panel by another is not incorporated into this simple panel model. Finer detail of the spacecraft surface, such as protruding antennae, star camera baffles, are either neglected or can be handled by slightly adjusting the parameters of the larger flat surfaces.

For such panel models, the radiation pressure force coefficient vector for the entire spacecraft can be computed by simply summing the panel contributions, as follows:

$$C_{\mathrm{r}} = \sum_i C_{\mathrm{r},i} \tag{5}$$

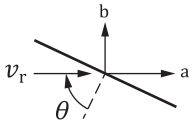

a Drag.

b Lift.

Figure 23 — Lift and drag directions with respect to the relative wind direction for flat plate model

For calculating the aerodynamic force coefficient using such a panel model, a double summation is necessary, both over the spacecraft panels *i*, and over the atmospheric constituents *j*. In addition, the contributions of drag and lift were computed separately, and now need to be summed as well.

$$\bar{C}_{\mathrm{a}} = \sum_i \sum_j \left(\frac{\rho_j}{\rho}\right)\left(C_{\mathrm{D},i,j}\hat{u}_{\mathrm{D}} + C_{\mathrm{L},i,j}\hat{u}_{\mathrm{L},i}\right) \tag{6}$$

where $\left(\frac{\rho_j}{\rho}\right)$ represents the relative mass concentrations of the different particles species (j = O_2, N_2, O, He, H, . . .) having different molecular masses m_j. The drag direction $\hat{u}_{\mathrm{D}}$ is determined from the relative velocity vector v_{r} as:

$$\hat{u}_{\mathrm{D}} = \frac{v_{\mathrm{r}}}{\| v_{\mathrm{r}} \|} \tag{7}$$

The unit vector for the lift and side force direction, $\hat{u}_{\mathrm{L},i}$, is perpendicular to $\hat{u}_{\mathrm{D}}$ and in the plane spanned by $\hat{n}_i$ (normal to panel i) and $\hat{u}_{\mathrm{D}}$.

$$\hat{u}_{\mathrm{L},i} = -\frac{\left(\hat{u}_{\mathrm{D}} \times \hat{n}_i\right) \times \hat{u}_{\mathrm{D}}}{\| \left(\hat{u}_{\mathrm{D}} \times \hat{n}_i\right) \times \hat{u}_{\mathrm{D}} \|} \tag{8}$$

Drag and lift coefficients can be determined from:

$C_{\mathrm{D}} = \bar{C}_{\mathrm{a}} \cdot \hat{u}_{\mathrm{D}}$ and $C_{\mathrm{L}} = \left|\bar{C}_{\mathrm{a}} - C_{\mathrm{D}}\hat{u}_{\mathrm{D}}\right|$, with lift being in the unit direction of $\frac{\bar{C}_{\mathrm{a}} - C_{\mathrm{D}}\hat{u}_{\mathrm{D}}}{\left|\bar{C}_{\mathrm{a}} - C_{\mathrm{D}}\hat{u}_{\mathrm{D}}\right|}$ (lift can be zero, such that the programmer shall guard against division by zero in this last formula).

As necessary inputs to Formulae (5) to (8), each panel's drag coefficient and combined lift and side force coefficient are determined from:

$$C_{\mathrm{D},i,j} = \left[\frac{P_{i,j}}{\sqrt{\pi}} + \gamma_i Q_j Z_{i,j} + \frac{\gamma_i}{2}\frac{v_{\mathrm{re}}}{v_{\mathrm{inc}}}\left(\gamma_i \sqrt{\pi} Z_{i,j} + P_{i,j}\right)\right]\frac{A_i}{A_{\mathrm{ref}}} \tag{9}$$

$$C_{\mathrm{L},i,j} = \left[l_i G_j Z_{i,j} + \frac{l_i}{2} \frac{v_{\mathrm{re}}}{v_{\mathrm{inc}}} \left(\gamma_i \sqrt{\pi} Z_{i,j} + P_{i,j} \right) \right] \frac{A_i}{A_{\mathrm{ref}}} \tag{10}$$

where

$$\gamma_i = \cos\left(\theta_i\right) = -\hat{u}_{\mathrm{D}} \cdot \hat{n}_i \tag{11}$$

$$l_i = -\hat{u}_{\mathrm{L}} \cdot \hat{n}_i \tag{12}$$

$$S_j = \frac{v_{\mathrm{r}}}{\sqrt{2\left(\frac{R}{0{,}001\, m_j\,(u)} \right) T}} \tag{13}$$

$$G_j = \frac{1}{2S_j^2} \tag{14}$$

$$P_{i,j} = \frac{1}{S_j} e^{-\gamma_i^2 S_j^2} \tag{15}$$

$$Q_j = 1 + G_j \tag{16}$$

$$Z_{i,j} = 1 + \mathrm{erf}\left(\gamma_i S_j\right) \tag{17}$$

$$\frac{v_{\mathrm{re}}}{v_{\mathrm{inc}}} = \sqrt{\frac{1}{2}\left[1 + \propto \left(\frac{4RT_{\mathrm{W}}}{0{,}001\, \mathrm{m}_j\,(u)\, {v_{\mathrm{r}}}^2} - 1 \right) \right]} \tag{18}$$

A_{ref} is the reference area of the spacecraft in square meters and should be a positive constant during the whole computation of drag on a panel model. An averaged spacecraft cross-sectional area is commonly adopted for A_{ref}.

Also, $\propto$ is the accommodation coefficient, T_{W} is the wall temperature in K, R is the universal gas constant in $\frac{\mathrm{J}}{\mathrm{K\,mol}}$, and v_{r} is the relative velocity in m/s.

The unit vector in the drag direction depends only on the relative velocity and is independent of the panel orientation, and therefore does not carry the index *i*. Depending on the orientation of the 2D panel within the 3D spacecraft model, the lift contribution of each panel, in the direction $\hat{u}_{\mathrm{L},i}$ shall result in a combined aerodynamic lift and side force.

As an example, the aerodynamic force coefficient for a single plate having an area of 1,0 m^2 is examined. Next, three panel angles of incidence with reference to the drag vector (i.e. θ_i, the angle between the panel inward normal and the drag vector of 0°, 45° and 90°) as depicted in Figure 24. For this example, the conditions and accompanying configurations shown in Table 5 are examined for only the oxygen component:

$$A_{\mathrm{ref}} = 1, \quad T_{\mathrm{W}} = 300, \quad R = 8{,}314\,462\,1, \quad \propto = 1, \quad T = 1\,000, \; m_j = 16\,\mathrm{u}\ (\text{atomic ¿xygen})$$

$$v_{\mathrm{r}} = 7\,600$$

Table 5 — Lift and drag coefficient results for three test cases

Parameter	$\theta_i = 0°$	$\theta_i = 45°$	$\theta_i = 90°$
γ_i	1,0	0,707 106 78	0,0
l_i	0,0	0,707 106 78	1,0
S_j	7,454 894	7,454 894	7,454 894
G_j	0,008 996 8	0,008 996 8	0,008 996 8
$P_{i,j}$	9,805e-26	1,146 84e-13	0,134 140 06
Q_j	1,008 996 8	1,008 996 8	1,008 996 8
$Z_{i,j}$	2,0	1,999 999	1,0
$\frac{v_{re}}{v_{inc}}$	0,073 471 5	0,073 471 5	0,073 471 5
$C_{D,i,j}$	2,148 218 46	1,492 049	0,075 680 4
$C_{L,i,j}$	0	0,077 835 82	0,013 924 5

The C_D and C_L profiles associated with this test case, as reported by Doornbos,[43] are shown in Figure 24. The constituent data in the example contained in Table 5 match the Doornbos C_D and C_L values for oxygen.

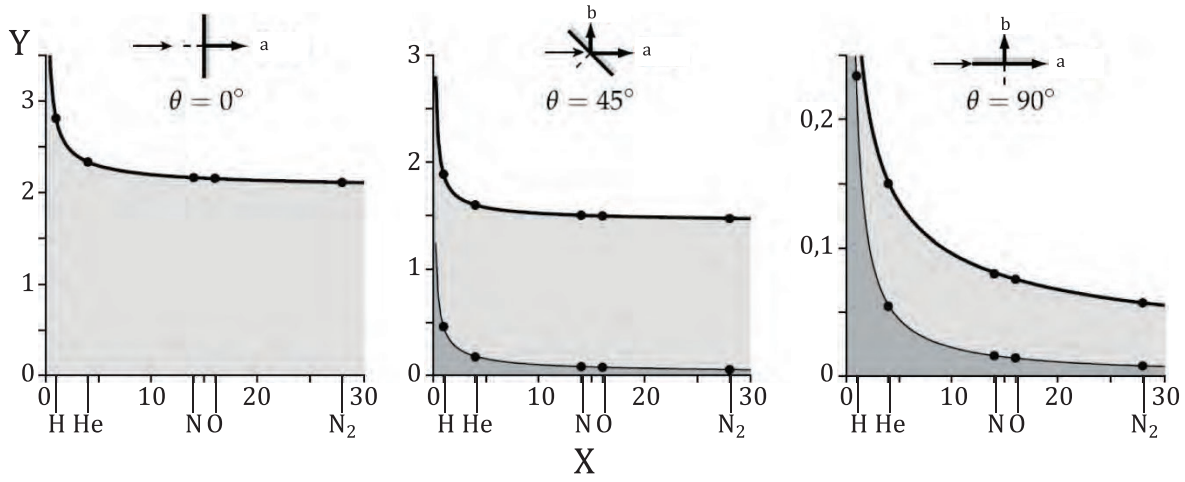

Key

X mass of gas particles (u)

Y drag and lift coefficient

a Drag.

b Lift.

Figure 24 — Variation of drag and lift coefficients for one-sided panel as function of gas constituent

Another viable approach to drag coefficient modelling is to establish a reference C_D = f (altitude) law comprised of a mean cross-sectional area (C_{Dmean}) hypothesis.[9] It is based on the value of the drag coefficient of a plate in tumbling mode.

Higher-fidelity approaches to drag coefficient estimation are also found in literature.[44] More accurate aerodynamic and radiation pressure coefficient estimation techniques do exist based upon detailed 3D geometry models with an arbitrary number of precisely positioned and shaped panels. For example, specialized software such as ANGARA [46] is based on CAD drawings of the space object. ANGARA is able to calculate both radiation pressure and aerodynamic force coefficients using the same tools for building the spacecraft geometry. Similar techniques and software implementations are described in References [47], [48], [49] for radiation pressure effects and in Reference [45] for aerodynamics.

8.2.3 Hypersonic rarefied gas flow adjustments via the Knudsen number and other considerations

When an object (even a simple flat plate) passes through rarefied gases and the body temperature is low, the thermal speed at which the impacting molecules are re-emitted from the surface can be low compared to the flat plate speed. This results in an accumulation of molecules on the upwind side of the flat plate which in turn interacts with the incident-free flow of molecules and affects the orbit lifetime calculation by altering the kinetic energies of impacting molecules. The magnitude of this effect can be characterized by the Knudsen number, which is the ratio between the molecular mean free path and plate thickness.

While it is often thought that this free molecular flow approximation is sufficient, this is not always true due to thermal accommodation of molecules at satellite wall. The Knudsen number can be very large at high altitude since the free flow mean free path of molecules large, yet it does not always fairly represent what occurs near to the surface. This is especially true for slowly-reflected molecules due to low plate temperature and for non-convex space object shapes (imagine two flat plates joined at an obtuse angle, where molecules from impingement on one plate encounter are reemitted from the other plate into free flow, causing a local interaction similar to a shock wave, thereby changing the nature of the pressure exerted locally on the satellite surface and its resulting drag). These effects can be addressed with using numeric approaches dedicated to the hypersonic rarefied gas flows, such as direct simulation Monte Carlo (DSMC) methods[46].

8.3 Estimating cross-sectional area with tumbling and stabilization modes

If the simple panel model described in 8.2.2 is used or a more sophisticated drag coefficient estimation technique was selected coupled with a fixed reference area, then the ballistic coefficient shall use the reference area which accompanies the estimated drag coefficient.

Conversely, if a static drag coefficient was selected in 8.2.2, then cross-sectional variations shall be incorporated into the ballistic coefficient for asymmetric objects. The ballistic coefficient has a sensitive impact on the orbit lifetime. Average cross-sectional area is one of three key components (the others being mass and drag coefficient) which comprise the ballistic coefficient. In this subclause, methods used to estimate average cross-sectional area are examined.

If the attitude of the spacecraft can't be anticipated (as is typically the case), the user shall compute a mean cross-sectional area assuming that the attitude of the spacecraft varies uniformly (relatively to the velocity direction), i.e. that all the possible attitudes can be achieved with the same probability and during the same time. The mean cross-sectional area is obtained by integrating the cross-sectional area across a uniform distribution of attitude of the spacecraft (as if an observer would observe a spacecraft from any direction and compute the resulting mean observed cross-section).

In the absence of a more detailed model, a composite flat-plate model can be utilized. For example, for a plane sheet of which S is the area, it can be demonstrated that the "mean surface area" is S/2 when averaged over all possible viewing angles; by extension, for a parallelepiped-shaped spacecraft, S1, S2, S3 being the three surfaces (their opposite sides are to be neglected because when a side is visible, the opposite one is masked), it can be demonstrated that this "mean surface area" is (S1+S2+S3)/2; if a solar array of surface S4 is added, the mean surface area is then (S1+S2+S3+S4)/2 (neglecting any possible masking between the solar array and the spacecraft). This flat plate model has been shown to be accurate to within 20 % for tracked objects. Since masking effects represent a systematic bias that has the effect of reducing drag (thereby increasing orbit lifetime), an appropriately conservative cross-sectional area masking reduction factor shall be introduced to maintain accuracy.

To eliminate the need for such conservatism, this plate model approach can be extensively refined by integrating the cross-sectional area of the spacecraft across all anticipated tumbling attitudes (e.g. using a computer-aided design or CAD program), and then dividing the result by the difference between the limits of integration. The analyst is then left with a properly weighted average cross-sectional area.

For space objects with a large length to diameter ratio, the analyst shall consider whether gravity gradient stabilization will occur and adjust the cross-sectional area based upon the anticipated stabilized geometry. Similarly, for space objects which have a large aero-torque moment (i.e., the centre-of-gravity and centre-of-pressure are suitably far apart and the aerodynamic force is suitably large), the analyst shall consider whether the spacecraft would experience drag-induced passive attitude stabilization and adjust the cross-sectional area accordingly.

8.4 Estimating mass

The mass of the spacecraft shall be assumed to be its total mass at mission completion, where total mass is comprised of the spacecraft's dry mass plus the anticipated fuel margin of safety upon completion of the spacecraft's deorbit or safing manoeuvres. Such fuel margin/mass can be neglected if venting is planned prior to end of the deorbit phase (e.g. for an upper-stage).

Annex A
(informative)

Space population distribution

The launch vehicle and its family of deployed objects pass through various orbit regimes during the ascent phase from launch up to the mission orbit. As can be seen in Figure A.1 through Figure A.4, the collision risk is especially high in specific orbital regimes (the LEO and GEO belts and at the altitudes of deployed constellations).

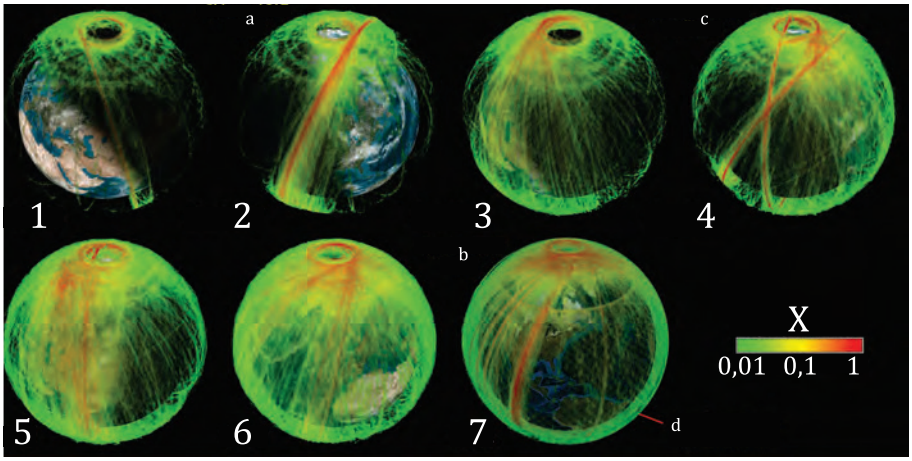

Key

X objects per million km^3
1 jan 2005
2 mar 2007
3 jan 2009
4 apr 2009
5 2010
6 2017
7 2021
a Chinese ASAT test.
b Russian ASAT test.
c Iridium/Cosmos collision.
d New Space Large Constellations.

Figure A.1 — Evolution of near-earth space spatial density, 2005 - 2021

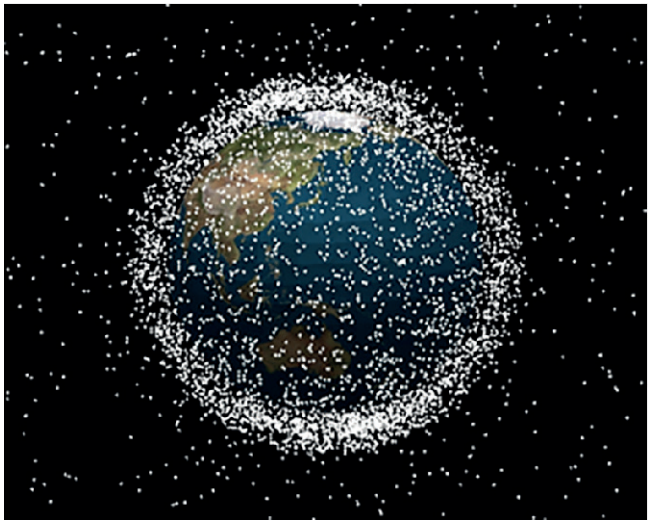

Figure A.2 — Distribution in low Earth orbit

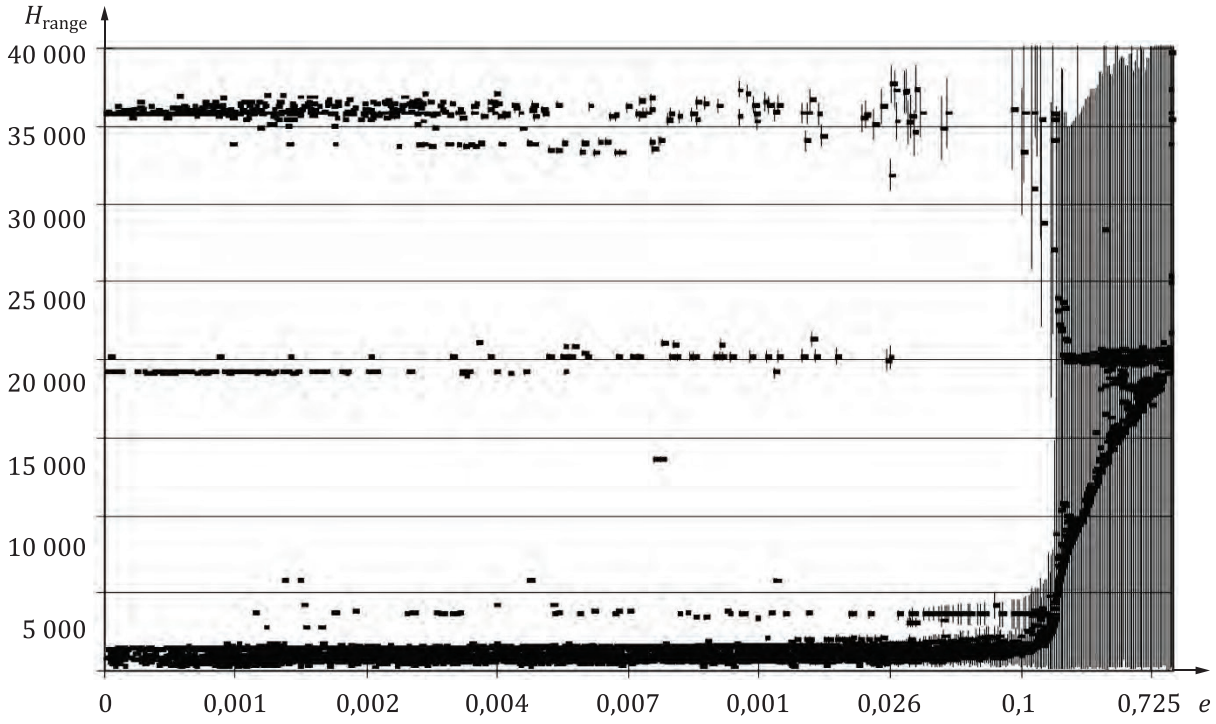

Key

e orbit eccentricity

H_{range} range of altitudes occupied by space objects

Figure A.3 — Space population by altitude and eccentricity

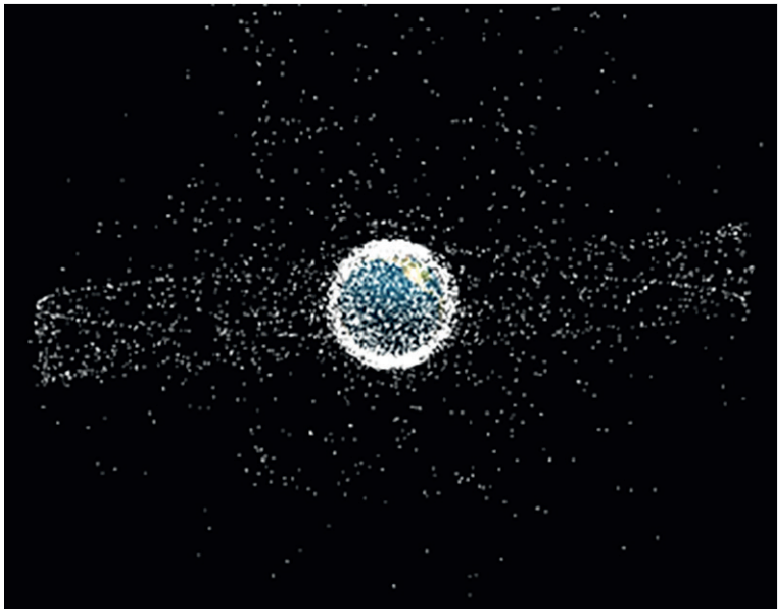

Figure A.4 — Distribution in near-Earth space

Annex B
(informative)

25-year lifetime predictions using random draw approach

If the user of this document wishes to estimate whether a space object has a 25-year orbit lifetime or not, a set of method 3 analysis products have been generated and are available in this annex. This method 3 data were generating utilizing solar/geomagnetic modelling approach #1, coupled with a method 2 orbit lifetime analysis tool (1Earth Research semi-analytic orbit propagator 'QPROP'). QPROP was used to examine the 8 million cases contained in Table B.1, spanning a variety of times-into-the-solar-cycle, inclinations, perigee altitudes (H_p), apogee altitudes (H_a), and ballistic coefficients. QPROP uses semi-analytic propagation of mean orbit elements coupled with gravity zonals J_2 and J_3 and selected atmosphere models (including NRLMSISE-00, Jacchia-Bowman, Jacchia 1971, etc). QPROP has been used to analyse orbit lifetime and spacecraft re-entry by several Government and industrial organizations. Its accuracy has been validated by high-precision numerical integration results (method 1 type).

Table B.1 — QPROP grid of test cases

Parameter	Lower limit	Upper limit	Step size
Time into solar cycle (days)	0	2 964,75	3 953/4
Inclination (°)	0	90	30
β (cm^2/kg)	25	500	25.
Perigee altitude (km)	100	2 000	50
Apogee altitude (km)	250.	10 000	50
Number of trials	0	3	1

The primary independent variables of the orbit lifetime estimation process are contained in Table B.1. By stepping through all of these variables in the ranges and step sizes indicated in the table, and then detecting those cases which resulted in a 25-year orbit lifetime, the dependencies between ballistic coefficient and orbit initial condition can be found. While both the NRLMSISE-00 and Jacchia-Bowman atmosphere models are implemented in QPROP, the NRLMSISE-00 model was used for these analyses due to its faster runtime with similar long-term propagation accuracy. Random draws of the triad of solar and geomagnetic index parameters (see 5.3) were implemented. To capture variations exhibited by the random draw process, a number of trials were used (four, in this case).

For a spacecraft having a ballistic coefficient of 200 cm^2/kg and starting in a circular, equatorial orbit at the altitude shown, Figure B.1 depicts the resultant ranges of anticipated orbit lifetime. The 'minimum' and 'maximum' incorporates the entire range of orbit decay start times with respect to the solar cycle minimum. The right-hand side of the plot shows how variable the results can get in the neighbourhood of 25 years estimated lifetime.

The dependence of orbit lifetime upon orbit inclination is shown for the same 200 cm^2/kg sample case in Figure B.1 and Figure B.2, where it is seen that polar orbits experience reduced atmospheric drag, likely due to both the reduced time spent flying near the solar sub-point in combination with the reduced atmospheric density at the Earth's poles due to the oblate shape of the Earth and atmosphere.

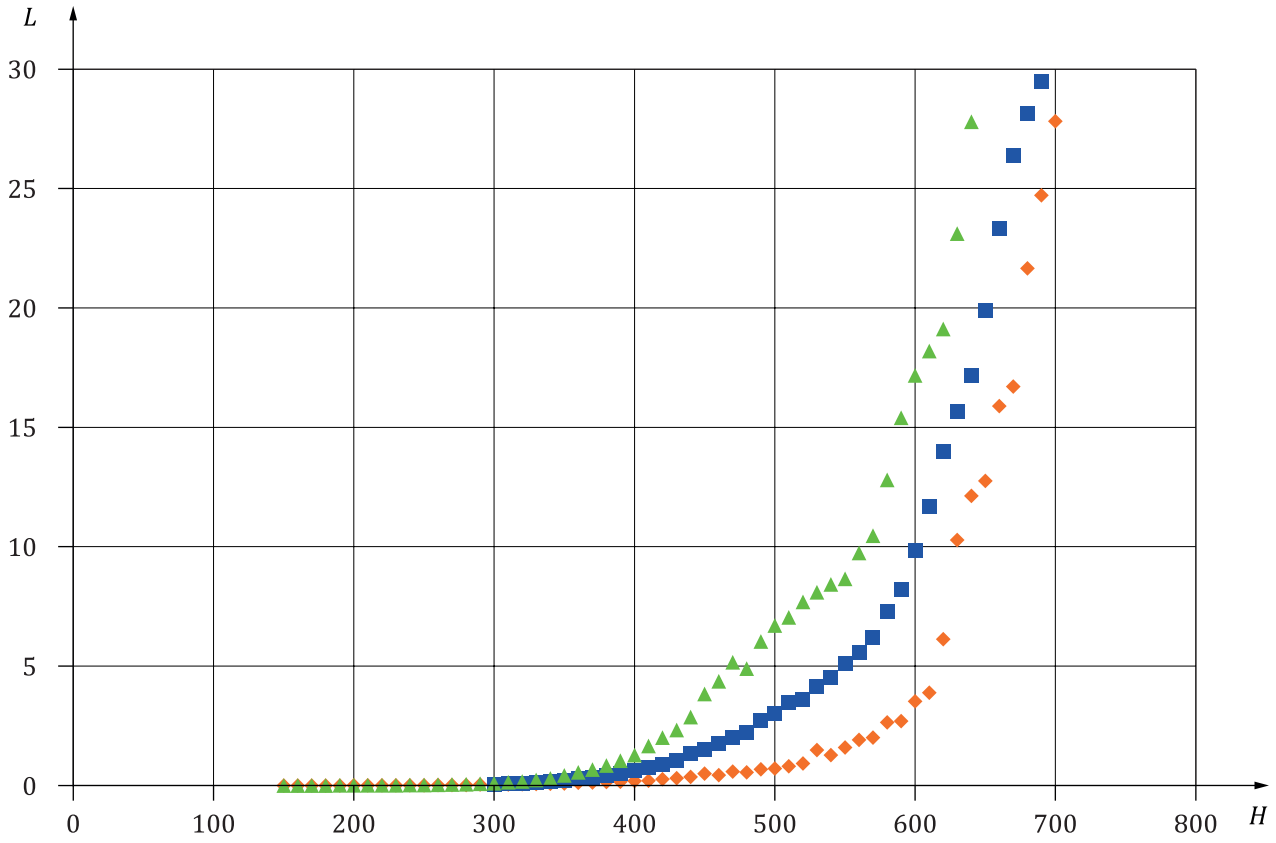

Key

H	circular orbit altitude, expressed in km
L	orbit lifetime, expressed in years
◆	minimum orbit lifetime
■	typical orbit lifetime
▲	maximum orbit lifetime

Figure B.1 — Sample orbit lifetime (β = 200 cm^2/kg, equatorial orbit) as a function of initial orbit altitude

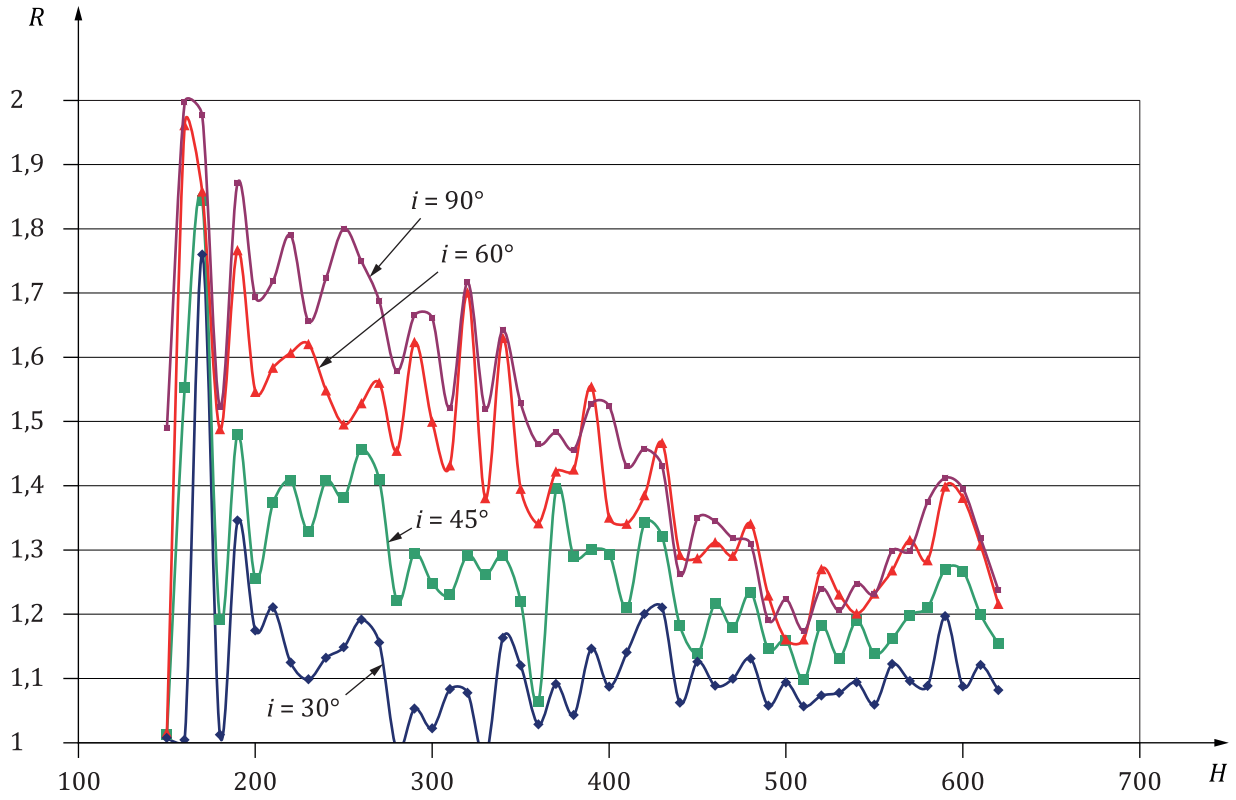

Key

H circular orbit altitude, expressed in km

R ratio of inclined orbit lifetime to equatorial

Figure B.2 — Orbit lifetime dependence upon orbit inclination

Future studies can use more trials and incorporate finer step sizes, but the large computer runtime requirements of these many cases led to the initial selection of 4 trials per initial set of orbit conditions. Through extensive simulation, it was found for non-Sun-synchronous orbits that orbit lifetime results are not sensitive to the three angular orbit elements (RAAN, argument of perigee and mean anomaly) and therefore the three initial values are arbitrarily chosen and assumed for all cases. The sensitivity to RAAN and argument of perigee can be significant for sun-synchronous, and more generally for high-eccentricity orbits; this was discussed in subclause Orbit lifetime statistical approach for high-eccentricity orbits (e.g. GTO) 5.6. Sun-synchronous orbit cases should be studied using a 'method 1' or '2' approach; until such time as their orbit lifetimes can be appropriately categorized in graphical and/or functional form. Further, it was found that orbits having inclinations greater than 90 degrees can be well-represented by the pole-symmetric orbits having complementary orbit inclinations (justifying analysis of only 0° to 90° as shown in Table B.1).

The shaded regions shown in Figure B.3 and Figure B.4 denote the categorization of the orbit initial conditions at the start of the orbit decay with respect to the 25-year post-mission lifetime constraint specified in ISO 24113. Region 1 denotes orbit initial conditions which will result in an orbit lifetime shorter than 25 years (in all observed cases). Region 2 denotes initial orbit conditions that can result in an orbit lifetime that is greater than the recommended 25-year limit, in certain circumstances. Figure B.3 and Figure B.4 were generated using a parametric sampling of starting conditions, and uncertainties in lifetime are not shown in the plots.

One can observe from Figure B.3, Figure B.4, and Figure B.5 that there are a wide variety of initial orbit, timing, solar and geomagnetic conditions which can combine to produce an orbit lifetime of 25 years. Figure B.3, Figure B.4, and Figure B.5, while helpful, still leave the user with uncertain knowledge of what the post-mission orbit lifetime will be specific to their initial conditions. Fortunately, the results of the 7,68 million analyses have been retained[6]; interpolation of these results is possible to predict orbit lifetime for a specific set of initial conditions. And, to the extent that 4 sets of random draw cases is not necessarily

an exhaustive analysis, additional cases can be run to further refine the orbit lifetime estimation grid and improve interpolation results.

Orbit lifetime data generated by the many analysis runs can be fit with a set of analytical expressions which predict average orbit lifetime (in years) as a function of H_p, inclination, ballistic coefficient and orbit eccentricity.[6] However, the resulting set of equations exhibits a peak deviation of up to 100 % from the underlying estimated lifetime data in extreme cases, coupled with an average standard deviation of less than 20 % error above 200 km. The effort invested in obtaining this unsuitable result indicates that a better approach would be to not fit the data, but rather to:

a) use the method 2 analysis tool to entirely map out the orbital lifetime topography[50];

b) store the lifetime topography data electronically;

c) provide space operators with a simple and fast electronic access to a topography interpolation function.

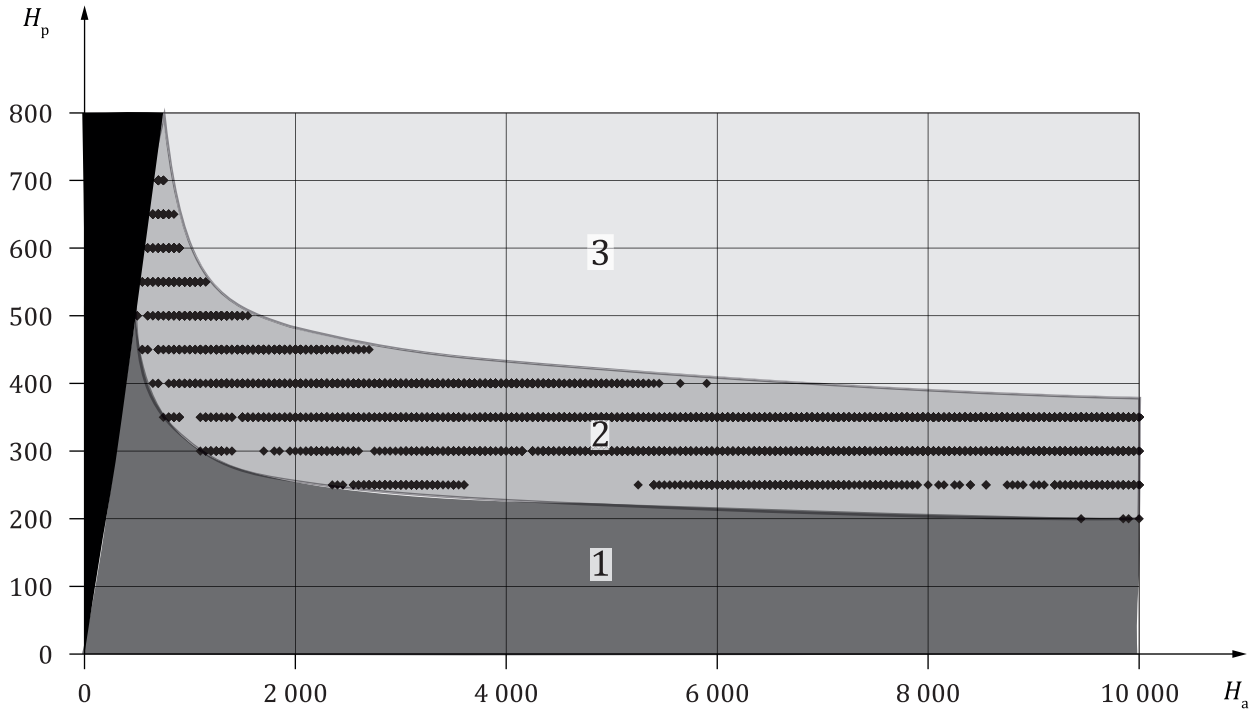

Key

H_a apogee altitude, expressed in km

H_p perigee altitude, expressed in km

1 < 25 years

2 can be 25 years

3 > 25 years

Figure B.3 — Perigee versus apogee boundaries for 25-year orbit lifetime conditions (25 cm²/kg < β < 500 cm²/kg)

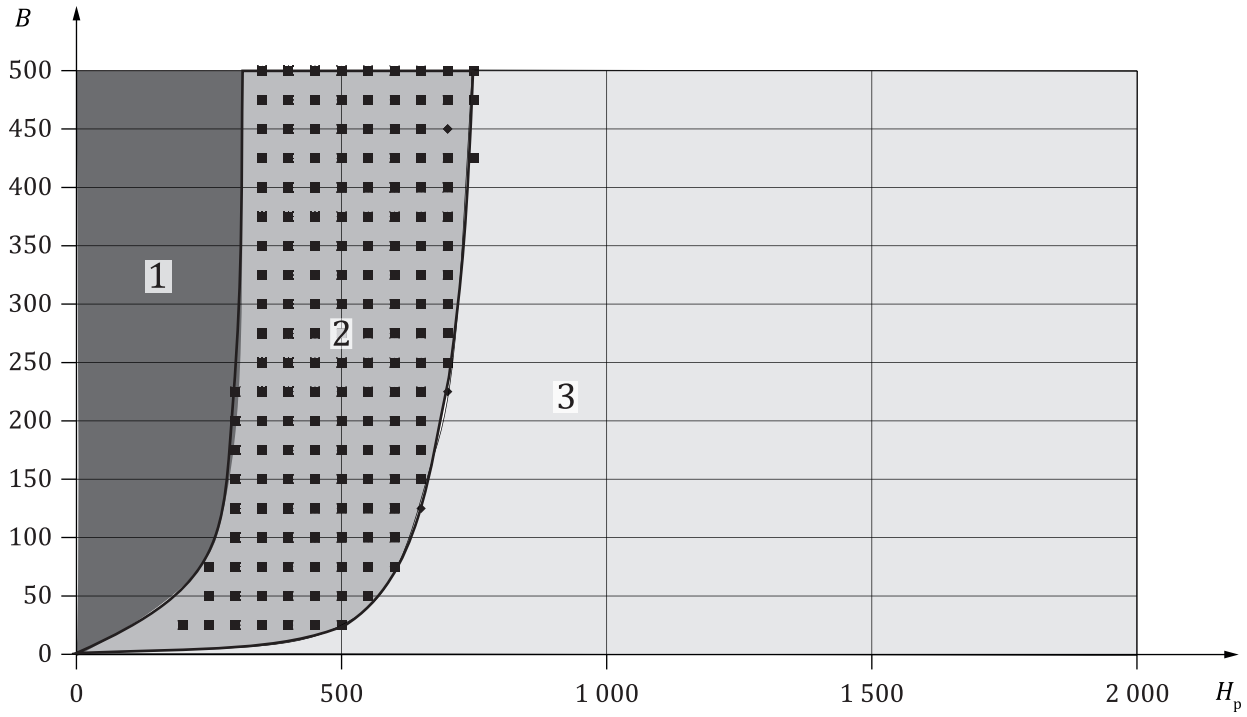

Key

H_p	circular orbit altitude, expressed in km
B	orbit lifetime, expressed in years
◆	inclination = 0 degrees
■	inclination = 30 degrees
▲	inclination = 60 degrees
×	inclination = 90 degrees
1	<25 years
2	can be 25 years
3	>25 years

Figure B.4 — Ballistic coefficient versus initial perigee altitude for all cases exhibiting 25-year orbit lifetime (apogee assumed < 10 000 km)

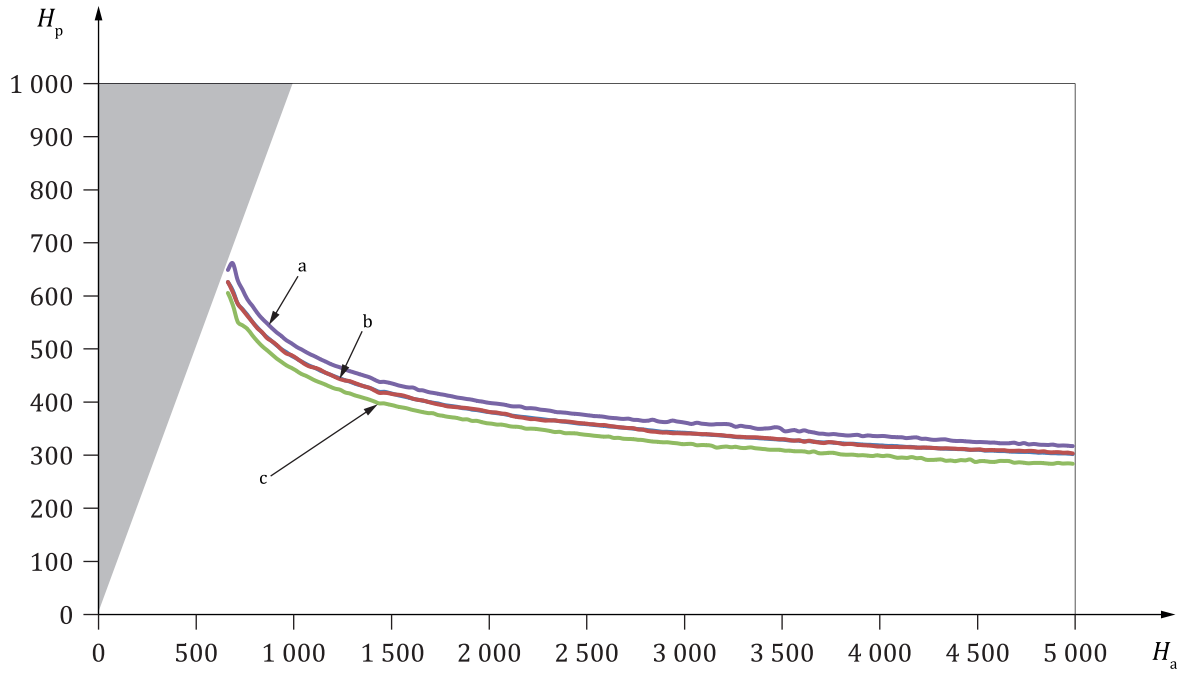

Key

H_a apogee altitude yielding 25-year lifetime, expressed in km

H_p perigee altitude yielding 25-year lifetime, expressed in km

a Maximum perigee for 25-year lifetime.

b Median perigee for 25-year lifetime.

c Minimum perigee for 25-year lifetime.

Figure B.5 — Orbit altitudes yielding a median 25-year orbit Lifetime for ballistic coefficient of 181,6 cm^2/kg using the MSIS atmosphere model and random draws of solar and geomagnetic data triads

Annex C
(informative)

Solar radiation pressure and 3rd-body perturbations

C.1 Solar radiation pressure modelling

For orbits with high eccentricity or high area-to-mass ratios, it is recommended that the analyst include perturbations due to solar radiation pressure (SRP). Several modelling resources can be found.[51] -[52] Implementations of such models can be checked against well-documented on-orbit observations. Figure C.1 shows variations in orbital elements for the Dash-2 spacecraft mission (1964), where the area-to-mass ratio was 37,9 cm^2/kg, with a reflectivity coefficient of 1,105, for an orbit inclination of 88,4 degrees, simulated using a method 1 numerical integration approach. As eccentricity and semi-major axis fluctuate due to SRP, perigee can become low enough in some cases that the spacecraft re-enters.

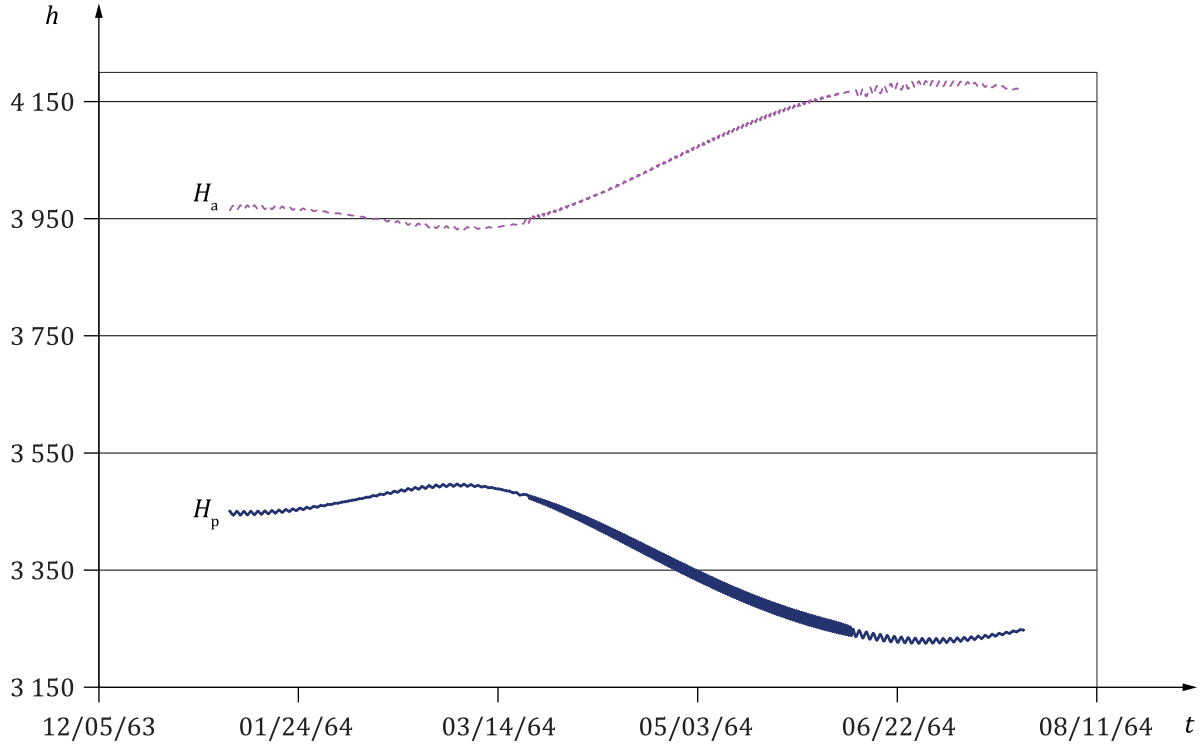

Key

t time, expressed as a date
h apsidal height, expressed in km
H_a apogee height
H_p perigee height

Figure C.1 — Perigee and apogee height versus time for SRP-induced variation in mean orbit elements for 1964 Dash-2 spacecraft

C.2 3rd-body modelling

Gravity contributions to the forces on an Earth-orbiting spacecraft are typically modelled using a gravity field for the Earth and point-mass third-body gravity forces arising from the Moon and Sun. Let B_i be a

celestial body and R_{Bi} locate its (centre-of-mass) position with respect to the inertial axes. The Newtonian formulae of motion [53] for a spacecraft are:

$$m\ddot{R} = F_S + \sum_{i=0} GmM_{Bi} \frac{R_{Bi} - R}{||R_{Bi} - R||^3} \tag{C.1}$$

where

m is the spacecraft mass

G is the universal gravitation constant

M_{Bi} is the mass of B_i

F_S is the sum of all forces on the spacecraft other than the point-mass gravitational force caused by all the celestial bodies (e.g. additional gravitational forces over the point-mass effect, drag, solar radiation pressure, general relativistic corrections).

The motions of the celestial bodies are taken to be known as a function of time, so that a suitable planetary ephemeris predictor is required to evaluate the third-body accelerations.

Bibliography

[1] Inter-Agency Space Debris Coordination Committee, “IADC Space Debris Mitigation Guidelines, Revision 3”, IADC-02-01, June 2021.

[2] Space Debris Mitigation Guidelines of the Scientific and Technical Subcommittee of the Committee on the Peaceful Uses of Outer Space, Annex IV of A/AC.105/890, p.42ff, 6 March 2007, endorsed by the United Nations General Assembly under Resolution A/RES/62/217 on 10 January 2008.

[3] Guidelines for the Long-term Sustainability of Outer Space Activities, A/AC.105/C.1/L.366, Guideline B.7.5.b, 17 July 2018, adopted by the United Nations General Assembly.

[4] ISO 23212, *Space systems — Detailed space debris mitigation requirements for spacecraft*

[5] ISO/TR 20590, *Space systems — Space debris mitigation design and operation manual for launch vehicle orbital stages [Tech Rpt]*

[6] OLTROGGE D.L. CHAO C.C. “Standardized Approaches for Estimating Orbit Lifetime after End-of-Life”, AAS/AIAA Astrodynamics Specialists Conference, Mackinac Island, MI, August 2007.

[7] KOZAI, Y., , “The Motion of a Close Earth Spacecraft”, Astronomical Journal **64**, 367—377, November 1959.

[8] Orbital Motion – 2nd Edition, ROY, A.E., Publ. by Adam Hilger, Ltd, Bristol, ISBN 0-85274-462-5, 1982.

[9] FRAYSSE, H. et al “Long term orbit propagation techniques developed in the frame of the French Space Act”. 22nd ISSFD, 2011.

[10] SHARMA, R.K. and al. “Lifetime estimation of upper stages reentering from GTO by genetic algorithm with response surface approximation”, IAC, 2006.

[11] LAMY, A. and al. “Analysis of Geostationary Transfer Orbit Long-Term Evolution and Lifetime”. 22nd ISSFD, 2011.

[12] BONNAL, C. and al. , “Space debris mitigation measures applied to European launchers”, Acta Astronautica **65** (2009) 1679–1688.

[13] FRAYSSE, H. and al. Statistical methods to address the compliance of GTO with the French Space Operations Act, 64th IAC, 2013.

[14] LAMY et al, “Resonance Effects on lifetime of Low Earth Orbit Satellites”, 23rd ISSFD,2012.

[15] LE FÈVRE, C. and al. “Compliance of disposal orbits with the French Space Act : the Good Practices and the STELA tool”, 63rd IAC, 2012 and Acta Astronautica Volume 94, Issue 1, January–February 2014, Pages 234–245.

[16] ANSI/AIAA Guide to Reference and Standard Atmosphere Models, ANSI/AIAA document #G-003B-2004.

[17] MARCOS F.A. BOWMAN B.R., SHEEHAN R.E. “Accuracy of Earth’s Thermospheric Neutral Density Models,” AIAA 2006-6167, AIAA/AAS Astrodynamics Specialist Conference, Keystone, Colorado, 2006.

[18] COMPARISON OF ATMOSPHERE MODELS FOR ATMOSPHERIC PREDICTIONS. 4th International Space Debris Re-entry Workshop, 28 Feb 2018.

[19] ISO/TR 11225, *Space environment (natural and artificial) — Guide to reference and standard atmosphere models*

[20] PICONE, J.M., HEDIN, A.E., DROB, D.P., AND AIKIN, A.C., , "NRL-MSISE-00 Empirical Model of the Atmosphere: Statistical Comparisons and Scientific Issues," J. Geophys. Res., doi:10.1029/2002JA009430, in press (2003).

[21] BOWMAN, B. R., TOBISKA, W. K., MARCOS, F. A., VALLARES, C., The JB2006 empirical thermospheric density model, Journal of Atmospheric and Solar-Terrestrial Physics **70** (5), 774-793, 2008.

[22] BOWMAN B.R. TOBISKA W.K., MARCOS F.A., HUANG C.Y., LIN C.S., BURKE W.J. New Empirical Thermospheric Density Model JB2008 Using New Solar and Geomagnetic Indices, AIAA 2008-6438, AIAA/AAS Astrodynamics Specialist Conference, Honolulu, Hawaii, August 2008.

[23] JUSTUS, C.G. AND LESLIE, F.W., The NASA MSFC Earth Global Reference Atmospheric Model—2007 Version, NASA/TM—2008–215581, November 2008.

[24] BRUINSMA S. THUILLIER G., BARLIER F. The DTM-2000 empirical thermosphere model with new data assimilation and constraints at lower boundary: accuracy and properties, Journal of atmospheric and solar-terrestrial physics ISSN 1364-6826, 2003, vol. 65, no. 9, pp. 1053-1070.

[25] CEFOLA, P., VOLKOV, I. I., SUEVALOV, V. V., Description of the Russian Upper Atmosphere Density Model GOST-2004, 37th COSPAR Scientific Assembly, Montreal, Canada, July, 2008.

[26] ISO 14222, *Space environment (natural and artificial) — Earth's atmosphere from ground level upward*

[27] Emmert, J. T., Drob, D. P., Picone, J. M., Siskind, D. E., Jones, M. Jr., Mlynczak, M. G., et al. (2020). NRLMSIS 2.0: A whole-atmosphere empirical model of temperature and neutral species densities. Earth and Space Science, 7, e2020EA001321. Accessible at: https://doi.org/10.1029/2020EA001321.

[28] "10.7-cm Solar Radio Flux (F10.7) data", downloadable at: ftp://ftp.seismo.nrcan.gc.ca/spaceweather/solar_flux/daily_flux_values/fluxtable.txt, format described at: ftp://ftp.seismo.nrcan.gc.ca/spaceweather/solar_flux/daily_flux_values/solarflux_eng.txt [cited 9 May 2022].

[29] Geomagnetic data, downloadable at: ftp://ftp.gfz-potsdam.de/pub/home/obs/kp-ap/wdc/yearly, format described at: ftp://ftp.gfz-potsdam.de/pub/home/obs/kp-ap/wdc/wdc_fmt.txt [cited 9 May 2022].

[30] WOODBURN. J., LYNCH, SHANNON, "A Numerical Study of Orbit Lifetime," AAS/AIAA Astrodynamics Specialists Conference, Lake Tahoe, AAS 05-297, 2005.

[31] LE FÈVRE, C. and al. "Orbit propagation and statistical methods to address the compliance of GTO with the French Space Operations Act", 6th IAASS, 2013.

[32] LE FÈVRE, C. and al. "Long term orbit propagation techniques developed in the frame of the French Space Act", 5th IAASS, 2011.

[33] FRAYSSE. H. and al. "STELA a tool for long term orbit propagation", International Conference on Astrodynamics Tools and Techniques, ESTEC-ESA, 2012.

[34] MORAND, V. and al. "Dynamical properties of Geostationary Transfer Orbits over long time scales: consequences for mission analysis and lifetime estimation" AIAA, 2012.

[35] MORAND, V., CAUBET, A. and al. "Semi analytical implementation of tesseral harmonics perturbations for high eccentricity orbits". AAS/AIAA, 2013.

[36] Matthes K., Funke B., Andersson M. E., Barnard L., Beer J., Charbonneau P. et al.2017). , Solar forcing for CMIP6 (v3.2). Geoscientific Model Development, **10**(6), 2247–2302. https://doi.org/10.5194/gmd-10-2247-2017.

[37] Solar forcing dataset for the Coupled Model Intercomparison Project 6, accessible at https://solarisheppa.geomar.de/cmip6

[38] MARCOS, F.A., WISE, J.O., KENDRA, M.J., GOSSBARD, N.J., BOWMAN, B.R., , "Detection of a long-term decrease in thermospheric neutral density," Geophysical Research Letters, Vol. **32**, L04103, doi:10.1029/2004GL021269, 2005.

[39] EMMERT J. T.2015), , Altitude and solar activity dependence of 1967–2005 thermospheric density trends derived from orbital drag, J. Geophys. Res. Space Physics, **120**, 2940–2950, doi:10.1002/2015JA021047.

[40] WENG L., LEI J., ZHONG J., DOU X., FANG H., 2020). A machine-learning approach to derive long-term trends of thermospheric density. Geophysical Research Letters, 47, e2020GL087140. https://doi.org/10.1029/2020GL087140.

[41] CNOSSEN I., 2022), A realistic projection of climate change in the upper atmosphere into the 21st century, Geophys. Res. Lett., 49, e2022GL100693, doi: 10.1029/2022GL100693.

[42] BROWN M.K., LEWIS H.G., KAVANAGH A.J., CNOSSEN I., 2021), Future decreases in thermospheric neutral density in low Earth orbit due to carbon dioxide emissions, J. Geophys. Res. Atmospheres, 126, e2021JD034589, doi: 10.1029/2021JD034589.

[43] DOORNBOS E., "Thermospheric density and wind determination from spacecraft dynamics," PhD Dissertation, Technical University of Delft, 25 March 2011.

[44] MEHTA P.M., MCLAUGHLIN C.A., SUTTON E.K., "Drag coefficient modelling for Grace using direct simulation monte carlo," COSPAR paper 0273-1177, 30 August 2013.

[45] FULLER John D., TOLSON Robert H.", Improved method for estimation of spacecraft free-molecular aerodynamic properties," Journal of Spacecraft and Rockets, **46**(5), 938–948, doi:10.2514/1.43205, 2009.

[46] FRITSCHE B., IVANOV M., KASHKOVSKY A., KOPPENWALLNER G., KUDRYAVTSEV A., VOSKOBOINIKOV U. et al., 1998), Radiation pressure forces on complex spacecraft, final report, ESOC contract 11908/96/D/IM, HTG, Germany and ITAM, Russia.

[47] ZIEBART M.", Generalized Analytical Solar Radiation Pressure Modeling Algorithm for Spacecraft of Complex Shape," Journal of Spacecraft and Rockets, Vol. **41**, No. 5, Sept.-Oct. 2004.

[48] Stuart Grey and Marek Ziebart, "Developments in High Fidelity Surface Force Models and their Relative Effects on Orbit Prediction." American Institute of Aeronautics and Astronautics.

[49] WETTERER C. J. et al., "Refining Space Object Radiation Pressure Modeling with Bidirectional Reflectance Distribution Functions," vol. 37, no. 1. American Institute of Aeronautics and Astronautics, pp. 185–196.

[50] FINKLEMAN D. OLTROGGE D. "Twenty-five Years, more or less: Interpretation of the LEO Debris Mitigation 25-Year Post-Mission Lifetime Guideline," AAS/AIAA Astrodynamics Specialist Conference, Toronto, Canada, 2010.

[51] AKSNES, K., "Short-Period and Long-Period Perturbations of a Spherical Spacecraft Due to Direct Solar Radiation," Center for Astrophysics, Harvard College Observatory and Smithsonian Astrophysical Observatory, Cambridge, Mass. 02138, U.S.A, 1975.

[52] Orbital Mechanics – 2nd Edition, CHOBOTOV, V.A., editor, AIAA Education Series, ISBN 1-56347-179-5, 1996.

[53] BERRY, M., AND COPPOLA, V.T, Correct Modeling of the Indirect Term for Third-Body Perturbations, AAS 07-417, 2007.

ICS 49.140
Price based on 48 pages

iso.org